International Applied Mechanics, Vol. 40, No. 12, 2004

FRACTURE AND STABILITY OF MATERIALS AND STRUCTURAL MEMBERS WITH CRACKS: APPROACHES AND RESULTS

A. N. Guz[1], M. Sh. Dyshel'[1], and V. M. Nazarenko[2]

UDC 539.3

A new alternative approach to fracture problems for materials and structural elements with cracks is set out. It is based on the mechanism of local instability near defects. The approach is used to study the fracture of materials compressed along interacting cracks and the fracture of thin structural members with cracks under tension with allowance for local buckling.

Keywords: new approach in fracture, crack, highly elastic composite, plastic material, structural member, panel, shell, tension, compression, stability

Introduction. The main question to answer by linear fracture mechanics, a well-established and widely accepted since, in looking into the possibility of further growth of existing cracks is whether the cumulative elastic energy is sufficient for additional surfaces of the defect to form. In Irwin's interpretation, this question is whether the integral characteristics of the stress–strain state at crack tips (stress intensity factors or crack opening displacement) achieve certain limit (critical) values under given loads.

In some cases, however, this approach is a fortiori inapplicable, though intuition suggests that fracture (crack growth or fragmentation) may (and will actually) occur under increasing loads. Among such cases is primarily loads acting along cracks—the stress intensity factors appearing in failure criteria such as the Griffith–Irwin one (linear fracture mechanics) are equal to zero, and, hence, fracture does not occur. The buckling of cracked materials (under compression along near-surface cracks parallel to the free surface) is a widely known and well-described phenomenon (in particular, in laminated composites). The aforementioned pertains equally to parallel cracks along which loads act.

It has long been known that local buckling triggers fracture [69]. Moreover, local buckling may strongly affect the classical linear fracture process by preceding it and frequently reducing the threshold levels of applied loads. This is particularly true of thin-walled structural members (plates and shells) where out-of-plane buckling precedes fracture.

This paper cites results of solving nonclassical problems of fracture mechanics where local buckling either triggers fracture (loads parallel to crack surfaces) or strongly influences the fracture process by preceding it and altering the geometry of the element (thin-walled plate or shell).

When the initial stresses are parallel to crack faces, there may be two classes of problems, depending on whether there is a field of additional stresses that are rather small compared with the initial stresses [8].

If there is no such an additional filed, then we deal with fracture under compression along cracks. The approach used to solve such problems is based on the relations of three-dimensional linearized solid mechanics. The concept of fracture is this: local buckling near cracks triggers fracture. The process of fracture is initiated when the initial stresses reach critical levels (values corresponding to local instability). This approach (including the relations of linearized solid mechanics, the corresponding mathematical tool, and failure criteria) is detailed in [8–12]. The formulation of the basic problems, methods for their solution, and results for plane cracks are addressed in the present paper.

[1]S. P. Timoshenko Institute of Mechanics, National Academy of Sciences of Ukraine, Kiev. [2]National University of Food Technology, Kiev, Ukraine. Translated from Prikladnaya Mekhanika, Vol. 40, No. 12, pp. 18–64, December 2004. Original article submitted December 22, 2003.

1063-7095/04/4012-1323

If there is an additional stress field, then we deal with brittle fracture of materials with initial stresses acting along cracks [8]. The approach is also based on the relations of three-dimensional linearized solid mechanics (the general formulation of fracture problems for prestressed materials is given in [8, 11, 12]). The approach assumes formulating failure criteria such as the Griffith–Irwin one (based on the integral characteristics of the additional field of initial stresses at crack tips), which are the classical criteria in the absence of initial stresses. These criteria in fact form the concept of fracture in this case: fracture sets in (a crack grows) when a certain combination of integral characteristics of the additional stress field at crack tips (namely, stress intensity factors) achieves a limit (critical) value. It should be noted that these factors depend on the initial stresses acting along cracks. Brittle-fracture problems for prestressed materials are beyond the scope of the present paper.

The paper [85] was the first to solve the stability problem for a rectangular linearly elastic isotropic plate with a central crack under uniaxial compression by an exact approach based on the three-dimensional linearized theory of stability of elastic bodies and by an approximate approach based on the beam approximation. These two approaches were used to determine the critical characteristics of the plate (dependence of the critical load on the crack parameter). The error of the beam approach was estimated.

Among fracture problems for materials compressed along cracks are those for cracked thin bodies (such as plates and shells) with local out-of-plane buckling in compression zones near cracks preceding traditional fracture (no buckling). The present paper cites results from an integrated study of the stress–strain state, stability, and fracture of plates and shells with cracks and crack-like defects.

1. Fracture of Materials Compressed along Crack-like Defects. We will classify the results to be discussed according to (i) the relative arrangement of defects (a single free crack in an infinite material, a near-surface crack parallel to the free boundary, two parallel internal cracks, and a periodic series of parallel cracks), (ii) loading conditions (uniaxial compression and biaxial uniform compression), and (iii) models of materials (hyperelastic materials with various elastic potentials, composite materials, and plastic materials). The above-listed ways the defects are arranged and, hence, interact with each other and with the free surface allow us to isolate, in a "pure" form, and study the following cases: interaction of a crack and the free surface of the material, interaction of two cracks, and interaction of a series of parallel cracks and to estimate the lower and upper bounds of the critical compressive stresses for a finite number of internal equidistant cracks.

Moreover, the analysis to be performed will make it possible to assess the limits of applicability of approximate approaches based on applied theories of beams, plates, and shells (such as a rigidly clamped strip isolated by cracks) [6, 33, 36]. Such an approximate approach, frequently called the beam approach, cannot be considered satisfactory for two reasons: (i) it is a fortiori inapplicable to cracks spaced rather far apart and (ii) it inadequately describes the situation near the edges of defects, idealizing it by introducing boundary conditions for a beam isolated by cracks. Generally, the boundary conditions are selected arbitrarily (rigid restraint, as a rule). Varying boundary conditions for, e.g., a strip from rigid restraint to simple support results in a four-fold change in the Euler critical compressive stress. For a more detailed analysis of issues associated with the beam approach, including its limits of applicability, see [17, 19, 24, 25, 29].

For each case of crack arrangement, we will formulate a boundary-value problem for one of the loading schemes and cite its exact solution (if any) or governing equations to which the problem is reduced. For a detailed discussion of the mathematical tool used, see the authors' works listed in references. On the whole, linearized boundary-value problems for cracked materials were attacked using methods of solving the Riemann–Hilbert problem (plane case), methods of potential theory (spatial case), the theory of integral Fourier and Hunkel transforms, and methods of solving dual integral equations by reducing them to systems of Fredholm equations of the first or second kind. A numerical eigenvalue analysis of systems of homogeneous integral equations was as a rule based on the Bubnov–Galerkin method.

For a closer look at studies on nonplanar cracks (cracks with cylindrical faces) see [32, 70, 71, 91]. The present paper does not discuss the results of such studies, because these interesting results, including the formulation of problems and the corresponding mathematics, deserve individual consideration. On the whole, the basic laws governing plane cracks remain for cylindrical cracks.

1.1. Free Cracks. A free cracks is meant a single crack in an infinite material. Note that a more general problem on a finite number of coplanar cracks (cracks lying in one plane) under either uniaxial compression or biaxial uniform compression has been solved in [8–10]. The critical compressive stresses corresponding to local instability near defects turned out to be the same as those for one crack. That is why coplanar cracks could be called free. Therefore, we will restrict ourselves to a plane problem for an infinite material with a single crack under uniaxial compression.

The stress–strain state of the material is homogeneous near cracks [8]:

$$\sigma_{ii}^0 = \text{const}, \quad \sigma_{22}^0 = 0, \quad \sigma_{11}^0 \neq 0, \quad \sigma_{33}^0 \neq 0,$$

$$u_m^0 = \delta_{im}(\lambda_i - 1)x_i, \quad \lambda_i = \text{const}, \quad \lambda_3 = 1 \quad (i = 1,2,3), \tag{1.1}$$

where λ_i are the strains along the axes, $\lambda_1 < 1$; δ_{ij} is the Kronecker delta; σ^0 and $\vec{u}^0$ are the stress tensor and displacement vector; and x_j are the Lagrange coordinates that coincide with the Cartesian coordinates in the undeformed state. The cracks are located in the plane $x_2 = \text{const}$ along the line of compression (axis x_1). We will mainly use the notation and terminology from [8].

At the initial stage of fracture under along-crack compression, the critical values of the parameters (λ_i or σ_{ii}^0) are determined, which correspond to local buckling near crack-like defects. Local instability is analyzed using the relations of linearized solid mechanics. With such an approach, problems of fracture under along-crack compression are linearized homogeneous boundary-value problems tested for eigenvalues with respect to the load parameters ($\lambda_1 < 1$ or $\sigma_{11}^0 < 0$ in crack planes). This remark pertains equally to spatial problems of fracture under uniform biaxial compression along cracks.

Due to symmetry about the crack plane, the problem reduces, by virtue of linearity, to problems for a half-space with symmetric and flexural buckling modes separately (i.e., for stress and strain fields symmetric and asymmetric about the crack plane). The boundary conditions (at $x_2 = 0$) of the plane problem for the lower half-plane $x_2 \leq 0$ are:

$$\widetilde{Q}_{22} = 0, \quad \widetilde{Q}_{21} = 0 \quad (y_1 \in L_2, \quad y_2 = 0)$$

$$\widetilde{Q}_{22} = 0, \quad u_1 = 0 \quad (y_1 \in L_2, \quad y_2 = 0) \tag{1.2}$$

for the flexural buckling mode and

$$\widetilde{Q}_{22} = 0, \quad \widetilde{Q}_{21} = 0 \quad (y_1 \in L_2, \quad y_2 = 0)$$

$$u_2 = 0, \quad \widetilde{Q}_{21} = 0 \quad (y_1 \in L_2, \quad y_2 = 0) \tag{1.3}$$

for the symmetric buckling mode.

Here the interval L_1 corresponds to the crack on the coordinate line y_1, and L_2 to the solid body (the points $y_2 = +\infty$ and $y_2 = -\infty$ are included in L_2); and $\widetilde{Q}$ and $\vec{u}$ are perturbations of the asymmetric stress tensor and displacement vector (the components $\widetilde{Q}$ are referred to the area of the body in the initial strain state). The boundary-value problem is formulated in coordinates y_j of the initial strain state related to the coordinates x_j of the undeformed state by

$$y_j = \lambda_j x_j. \tag{1.4}$$

Biaxial uniform compression along cracks located in the plane $x_3 = \text{const}$ induces the following homogeneous stress–strain state:

$$\sigma_{33}^0 = 0, \ \sigma_{11}^0 = \sigma_{22}^0 \neq 0, \ \sigma_{11}^0 = \text{const},$$

$$u_j^0 = \delta_{mj}(\lambda_j - 1)x_m, \quad \lambda_j = \text{const}, \quad \lambda_1 = \lambda_2 \neq \lambda_3, \quad \lambda_1 < 1. \tag{1.5}$$

The spatial problem reduces, as the plane one, to problems for flexural and symmetric buckling modes. The boundary conditions for the upper half-space $x_3 \geq 0$ (or $y_3 \geq 0$ in the coordinates of the initial strain state) are:

$$\widetilde{Q}_{33} = 0, \quad \widetilde{Q}_{31} = 0, \quad \widetilde{Q}_{32} = 0 \quad (\forall (y_1, y_2) \in S^*, \quad y_3 = 0)$$

$$\widetilde{Q}_{33} = 0, \quad u_1 = 0, \quad u_2 = 0 \quad (\forall (y_1, y_2) \notin S^*, \quad y_3 = 0) \tag{1.6}$$

for the flexural mode and

$$\widetilde{Q}_{33} = 0, \quad \widetilde{Q}_{31} = 0, \quad \widetilde{Q}_{32} = 0 \quad (\forall (y_1, y_2) \in S^*, \quad y_3 = 0)$$

$$u_3 = 0, \quad \widetilde{Q}_{31} = 0, \quad \widetilde{Q}_{32} = 0 \quad (\forall (y_1, y_2) \notin S^*, \quad y_3 = 0) \tag{1.7}$$

for the symmetric mode. Here S^* is the region occupied by the crack.

It was established that the initial stage of fracture in the case of an isolated crack is characterized by surface instability, i.e., critical strains and compressive stresses are equal to those in a half-space without cracks under surface instability. Moreover, the flexural and symmetric buckling modes give the same critical compressive stresses and strains.

The condition for determination of the critical strains, denoted by λ^* (and the corresponding compressive stresses by $\sigma^{0*} = \sigma^{0*}(\lambda^*)$), can be written in the following general form:

$$k(\lambda^*) = 0 \tag{1.8}$$

in the plane case and

$$q(\lambda^*) \cdot k(\lambda^*) = 0 \tag{1.9}$$

in the spatial case. Here

$$k = (l_1 - l_2) d_2 l_1^{-1} d_1^{-1} \tag{1.10}$$

for equal roots, $n_1 = n_2$, and

$$k = k_1 - k_2, \quad k_1 = l_1 n_2^{-1/2}, \quad k_2 = l_2 n_1^{-1/2} \tag{1.11}$$

for unequal roots, $n_1 \neq n_2$.

We have $\lambda^* = \lambda_1^*$ (and $\sigma_{11}^{0*} = \sigma_{11}^{0*}(\lambda_1^*)$) in the plane case (1.1) and $\lambda^* = \lambda_1^* = \lambda_2^*$ (and $\sigma_{11}^{0*} = \sigma_{11}^{0*}(\lambda_1^*)$, $\sigma_{11}^{0*} = \sigma_{22}^{0*}$), in the spatial case (1.5), $q = n_3^{-1/2} d_3$. The quantities $n_1, n_2, n_3, l_1, l_2, d_1, d_2$, and d_3 are determined by the components of the tensors ω and κ that relate the perturbations of the displacement vector $\vec{u}$ and the asymmetric Kirchhoff stress tensor t referred to the area of a compressible (tensor ω) or incompressible (tensor κ) body in undeformed state. The components of the tensors ω and κ depend on the chosen model of material and on the form of stress–strain state ((1.1) in the plane case or (1.2) in the spatial case). In particular, for hyperelastic materials the components of these tensors depend on the form of elastic potential. Moreover, the condition $k(\lambda^*) = 0$ determines the critical loads in the axisymmetric spatial case.

1.1.1. Highly Elastic Materials. The following critical strains λ_1^* have been obtained for hyperelastic materials:

Bartenev–Khazanovich potential [1] (incompressible body, equal roots):

$\lambda_1^* = 3^{-1/2} \approx 0.577$ for the plane problem (1.1)

and

$\lambda_1^* = \lambda_2^* = 3^{-1/3} \approx 0.693$ ($q \neq 0$) for the spatial problem (1.5).

Treloar potential [97] (incompressible neo-Hookean body, unequal roots):

$\lambda_1^* = -1/3 + \sqrt[3]{17/27 + \sqrt{11/27}} + \sqrt[3]{17/27 - \sqrt{11/27}} \approx 0.544$ for the plane problem (1.1)

and

$\lambda_1^* = \lambda_2^* = [-1/3 + \sqrt[3]{17/27 + \sqrt{11/27}} + \sqrt[3]{17/27 - \sqrt{11/27}}]^{2/3} \approx 0.666$ for the spatial problem (1.5).

Harmonic (*standard*) *potential* [95] (compressible body, equal roots):

$\lambda_1^* = 0.5$ for the plane problem (1.1)

and

$\lambda_1^* = \lambda_2^* = (1+\nu)/2$ (ν is a material constant)) for the spatial problem (1.5).

Note that in contrast to the Bartenev–Khazanovich and Treloar potentials, the critical loads for harmonic potential are greater in the axisymmetric case than in the nonaxisymmetric case: $\lambda_1^{ax^*} = (1+\nu)/(2+\nu) < \lambda_1^*$ (and $|\sigma_{11}^{ax*}| > |\sigma_{11}^{0*}|$), where the superscript "ax*" refers to the axisymmetric case.

1.1.2. Composite Materials. The critical stresses for composites have been determined in [8] using a continuum model with reduced characteristics of anisotropic (in particular, orthotropic or transversely isotropic) bodies with macrocracks, i.e., cracks much larger than the characteristic dimensions of structural elements of the composite. Since composites are relatively rigid at moderate temperatures, the second version of small subcritical deformation theory (as termed in [8]) was applied, where the initial state is determined by a geometrically linear theory. In this case, it is possible to neglect the difference between the coordinates of the undeformed and deformed states and quantities calculated in these coordinates.

The case of unequal roots (1.11) is characteristic of composites.

In the plane problem (1.1) for a composite material with reduced characteristics of an orthotropic body (with linear anisotropy), the critical stresses are determined from the equation

$$x^3\left[\frac{A_{22}}{A_{11}}\left(\frac{A_{22}}{A_{11}}-\varepsilon\right)\right]+x^2\left[\frac{A_{22}}{A_{11}}\left(\frac{A_{22}}{A_{11}}\varepsilon+2\frac{A_{22}}{A_{11}}-2\frac{A_{12}^2}{A_{11}^2}-\varepsilon\right)\right]$$

$$+x\left[\left(\frac{A_{22}}{A_{11}}-\frac{A_{12}^2}{A_{11}^2}\right)\left(\frac{A_{22}}{A_{11}}-\frac{A_{12}^2}{A_{11}^2}+2\frac{A_{22}}{A_{11}}\varepsilon\right)\right]+\left[\varepsilon\left(\frac{A_{22}}{A_{11}}-\frac{A_{12}^2}{A_{11}^2}\right)^2\right]=0,\quad x\equiv\frac{\sigma_{11}^0}{A_{11}},\quad \varepsilon\equiv\frac{G_{12}}{A_{11}},\tag{1.12}$$

where A_{ij} are the elastic coefficients and G_{ij} are the shear moduli.

Considering that the shear stiffness of composites is usually small ($\varepsilon \ll 1$), we can determine the minimum (in absolute value) negative root of Eq. (1.12) by the approximate formula

$$x\approx-\varepsilon\left[1-\varepsilon^2\left(\frac{A_{11}}{A_{22}}\right)\frac{A_{11}^2A_{22}^2}{(A_{11}A_{22}-A_{12}^2)^2}\right]=-\frac{G_{12}}{A_{11}}\left[1-\frac{G_{12}^2}{(A_{11}A_{22})}\frac{A_{12}^2A_{22}^2}{(A_{11}A_{22}-A_{12}^2)^2}\right].\tag{1.13}$$

Thus, the critical compressive stress can be determined from the formula

$$\sigma_{11}^{0*}\approx-G_{12}\left[1-\frac{G_{12}^2}{E_1E_2}(1-\nu_{13}\nu_{31})(1-\nu_{23}\nu_{32})\right].\tag{1.14}$$

Note that expression (1.14) represents the case of preferential reinforcement along cracks (macrocracks are oriented along reinforcement). For laminated materials this means that cracks are parallel to the interfaces between layers.

The critical stresses for a composite with reduced characteristics of a transversely isotropic medium follow from (1.13) as a special case on the assumption that cracks are in the plane of isotropy.

In the spatial problem (1.5) for a material with reduced characteristics of a transversely isotropic body (with linear anisotropy) (cracks are in the plane $x_3 = 0$), the critical stresses are determined from the equation

$$x^3\left[\frac{A_{33}}{A_{11}}\left(\frac{A_{33}}{A_{11}}-\varepsilon\right)\right]+x^2\left[\frac{A_{33}}{A_{11}}\left(\frac{A_{33}}{A_{11}}\varepsilon+2\frac{A_{33}}{A_{11}}-2\frac{A_{13}^2}{A_{11}^2}-\varepsilon\right)\right]$$

$$+x\left[\left(\frac{A_{33}}{A_{11}}-\frac{A_{13}^2}{A_{11}^2}\right)\left(\frac{A_{33}}{A_{11}}-\frac{A_{13}^2}{A_{11}^2}+2\frac{A_{33}}{A_{11}}\varepsilon\right)\right]+\left[\varepsilon\left(\frac{A_{33}}{A_{11}}-\frac{A_{13}^2}{A_{11}^2}\right)^2\right]=0,\quad x\equiv\frac{\sigma_{11}^0}{A_{11}},\quad \varepsilon\equiv\frac{G_{13}}{A_{11}}.\tag{1.15}$$

Considering that the shear stiffness of the composite is much smaller than the shear of planes parallel to the plane $x_3 = 0$, namely

$$\varepsilon=\frac{G_{13}}{A_{11}}\equiv\frac{G'}{E}\frac{(1+\nu)(1-\nu-2\nu'\nu'')}{(1-\nu'\nu'')}<1,\tag{1.16}$$

we can determine the minimum (in absolute value) negative critical stress (as a root of Eq. (1.15), denoted as in [25]) as

TABLE 1

$E^{(1)} / E^{(2)}$	E / G'	σ_{11}^{0*} / E	
		Exact value	Approximate value
1	2.600	–0.3308	–0.3375
4	3.828	–0.2386	–0.2408
7	5.408	–0.1743	–0.1751
10	7.023	–0.1364	–0.1367
13	8.648	–0.1117	–0.1119
16	10.278	–0.0946	–0.0947
19	11.911	–0.0820	–0.0820
22	13.545	–0.0723	–0.0724
25	15.180	–0.0647	–0.0647
28	16.815	–0.0585	–0.0585
31	18.452	–0.0534	–0.0534

$$\sigma_{11}^{0*} = \sigma_{22}^{0*} \approx -G'\left[1 - \frac{(G')^2}{EE'}(1-\nu^2)(1-\nu'\nu'')\right]. \tag{1.17}$$

Note that low shear stiffness is characteristic of laminated materials consisting of isotropic layers (interfaces are parallel to the plane $x_3 = 0$) and of fibrous composites with stochastic reinforcement in the planes $x_3 = \text{const}$ and weak reinforcement in the perpendicular direction.

The approximate formulas (1.14) and (1.17) are quite accurate. To prove this, Table 1 compares the exact solutions of Eq. (1.15) and approximate values of the critical compressive stress $\sigma_{11}^{0*} = \sigma_{22}^{0*}$ (normalized to the reduced elastic modulus E) obtained by formula (1.17) for different values of $E^{(1)} / E^{(2)}$ (the ratio of reduced characteristics E / G' is given for convenience). The data in the table represent a laminated composite with isotropic layers (a transversely isotropic medium in macrovolumes). Poisson's ratios of the layers are equal ($\nu^{(1)} = \nu^{(2)} = \nu = 0.3$) and the concentration of the material with the elastic modulus $E^{(1)}$ is $c_1 = 0.3$.

1.1.3. Plastic Materials. The critical stresses for plastic materials have been determined in [8].

In [8], by plastic fracture is meant a fracture process where total destruction is preceded by inelastic deformation (subcritical stress–strain states are homogeneous). The second version of small subcritical deformation theory is used, and it is possible to neglect the difference between the coordinates of the deformed and undeformed states and quantities calculated in these coordinates. Macrocracks, i.e., cracks larger than characteristic microstructures (grains, crystals, etc.) are considered. For elastoplastic materials, the characteristic equation has complex-conjugate roots $n_1 = \bar{n}_2$. The generalization of the mathematics to the case of complex-conjugate roots (and use of complex-valued functions of real variable) is discussed in [8, 25, 72].

An incompressible isotropic elastoplastic model was used to describe the deformation of the material. Specific results have been obtained for two most popular theories of plasticity: the deformation theory of plasticity and the associated flow rule.

TABLE 2

ε	σ_{11}^{0*} / E	
	Exact value	Approximate value
0.1	–0.176	–0.176
0.2	–0.204	–0.204
0.3	–0.228	–0.227
0.4	–0.247	–0.246
0.5	–0.263	–0.260
0.6	–0.275	–0.268
0.7	–0.285	–0.272
0.8	–0.293	–0.271
0.9	–0.299	–0.266
1.0	–0.304	–0.255

In the plane case (1.1), the critical compressive stresses σ_{11}^{0*} for a material described by the deformation theory of plasticity (small elastoplastic deformation theory) are determined from the equation

$$x^3 + \frac{8}{3}x^2\varepsilon + \frac{8}{9}x\varepsilon(1+2\varepsilon) + \frac{16}{27}\varepsilon^2 = 0, \quad x \equiv \frac{\sigma_{11}^0}{E_{\text{sec}}}, \quad \varepsilon \equiv \frac{E_{\tan}}{E_{\text{sec}}} < 1, \tag{1.18}$$

where E_{sec} and $E_{\tan}$ are the secant and tangent moduli on the diagram of stress intensity σ_i^0 versus strain intensity ε_i^0 (in particular, when $E_{\text{sec}} = E_{\tan}$, we have a linearly elastic incompressible body). Assuming ε small, we solve Eq. (1.18) by expanding x into a series in ε. For developed plastic strains ($\varepsilon << 1$), the minimum (in absolute value) negative root can be expressed accurate to ε^2:

$$x^* \approx -\frac{2}{3}\varepsilon\left(1 - \frac{1}{2}\varepsilon\right), \tag{1.19}$$

or

$$\sigma_{11}^{0*} \approx -\frac{2}{3}E_{\tan}\left(1 - \frac{1}{2}\frac{E_{\tan}}{E_{\text{sec}}}\right), \quad \varepsilon_{11}^{0*} \approx -\frac{1}{2}\frac{E_{\tan}}{E_{\text{sec}}}\left(1 - \frac{1}{2}\frac{E_{\tan}}{E_{\text{sec}}}\right) \quad (E_{\tan} < E_{\text{sec}}). \tag{1.20}$$

In the spatial case (1.5), both the deformation theory of plasticity and the associated flow rule were analyzed. For the deformation theory of plasticity, the equation for the critical stresses $\sigma_{11}^{0*} = \sigma_{22}^{0*}$ is

$$x^3 + \frac{2}{3}x^2(1+3\varepsilon) + \frac{x}{3}(1+3\varepsilon)(1+\varepsilon) + \frac{1}{27}(1+3\varepsilon)^2 = 0, \quad x \equiv \frac{\sigma_{11}^0}{E_{\text{sec}}}, \quad \varepsilon \equiv \frac{E_{\tan}}{E_{\text{sec}}}. \tag{1.21}$$

TABLE 3

Rock	$k_0 = 3k / E$	$c_0 = 3c / E$	σ_{11}^{0*} / E	
			Exact value	Approximate value
Mudstone ($\varepsilon = 0.198$)	$10.90 \cdot 10^{-3}$	3.048	–0.276	–0.278
Sandstone ($\varepsilon = 0.186$)	$15.07 \cdot 10^{-3}$	3.363	–0.278	–0.280

For structural materials ($|x| < 1$, $\varepsilon < 1$) with developed plastic strains, we may assume $\varepsilon << 1$. Therefore, the critical compressive stress can be determined from the approximate formula

$$\sigma_{11}^{0*} = \sigma_{22}^{0*} \approx -0.143 E_{\sec} \left[1 + 2.476 \frac{E_{\tan}}{E_{\sec}} - 1.692 \left(\frac{E_{\tan}}{E_{\sec}} \right)^2 \right]. \tag{1.22}$$

Table 2 compares the values of $\sigma_{11}^{0*} / E_{\sec}$ obtained as the exact solution of Eq. (1.21) and from the approximate formula (1.22) for different values of ε. As is seen, the approximate formula (1.22) describes well the solution for small values of ε and underestimates the root for ε close to unity (for $\varepsilon \le 0.7$ the difference between the exact and approximate values is less than 5%).

For the associated flow rule, an elementary loading function describing translational hardening (c and k are material constants) was considered,

$$f = (\hat{\sigma}_0^{\alpha\beta} - c\varepsilon_{p0}^{\alpha\beta})(\hat{\sigma}_{\alpha\beta}^0 - c\varepsilon_{\alpha\beta}^{p0}) - 2k^2 = 0, \tag{1.23}$$

where $\hat{\sigma}_0$ is the stress deviator; the critical compressive stresses $\sigma_{11}^{0*} = \sigma_{22}^{0*}$ are determined from the equation

$$x^3 + \frac{4}{3}(2 - 3\varepsilon)x^2 + \frac{4}{3}(1 - \varepsilon)(2 - 3\varepsilon)x + \frac{4}{27}(2 - 3\varepsilon)^2 = 0, \quad x \equiv \frac{\sigma_{11}^0}{E}, \quad \varepsilon \equiv \left(2 + \frac{3c}{E} \right)^{-1}. \tag{1.24}$$

Since ε is small for real materials, the approximate solution of the equation can be represented as

$$\sigma_{11}^{0*} \approx -0.304 E \left[1 - \frac{0{,}299}{(2 + c_0)} - \frac{0.628}{(2 + c_0)^2} \right], \quad c_0 \equiv \frac{3c}{E}. \tag{1.25}$$

The results from experiments on triaxial loading of mudstone and sandstone samples were used to determine the constants E, c, and k and the exact (Eq. (1.24)) and approximate (formula (1.25)) critical compressive stresses. These stresses normalized to the elastic modulus E are summarized in Table 3.

Thus, in the case of noninteracting cracks, the initial stage of fracture is associated with the surface instability of a half-space. For all the materials considered (hyperelastic materials with various elastic potentials, composite materials described by a continuum model with reduced characteristics, and plastic materials described by deformation theory and flow rule), the symmetric and flexural buckling modes have equal critical compressive stresses. The critical compressive stresses under biaxial uniform compression (spatial case) are less than those under uniaxial compression (plane case). In spatial problems, the critical stresses of the axisymmetric buckling mode are less than those of the nonaxisymmetric buckling mode. The exception is hyperelastic materials with a standard harmonic potential. The abnormal behavior of materials with a harmonic potential should be the subject of a separate investigation.

1.2. Near-Surface Cracks. This and next sections deal with interacting cracks: near-surface and internal cracks.

Near-surface cracks are parallel to the free boundary of the material. Considering this type of cracks, we can evaluate the interaction between a crack and the free surface under along-crack compression. Obviously, when the distance between the

free surface and the crack plane tends to infinity, the case at hand is a free crack, as in Sect. 1.1. If this distance is small, then the critical compressive stresses are much smaller than those for a free crack.

As for interacting internal cracks, two parallel cracks and a periodic series of equidistant cracks are the most interesting cases, since they give upper and lower estimates of the critical compressive stresses for the case of a finite number of internal equidistant cracks. Clearly, when the distance between cracks tends to infinity, we arrive at the case of noninteracting cracks.

Note that the critical compressive stresses of the axisymmetric buckling mode are less than those of the nonaxisymmetric buckling mode.

1.2.1. An Exemplary Formulation of a Boundary-Value Problem. Near-surface cracks were studied in [3–5, 22, 26, 27, 62–66, 69, 80, 93]. Let us formulate the spatial nonaxisymmetric problem (1.5) as an example [8].

Consider a crack of radius a located in the plane $x_3 = 0$ of the upper half-space $x_3 \ge -h$ with the center on the Ox_3-axis: $\{0 \le r < a,\ 0 \le \theta < 2\pi,\ x_3 = 0\}$ ((r, θ, x_3) are cylindrical coordinates derived from Cartesian coordinates). The crack faces and the half-space boundary are free from stresses. The boundary conditions of the linearized problem are

$$t_{3r} = 0, \quad t_{3\theta} = 0, \quad t_{33} = 0 \quad (x_3 = \pm 0, \quad r < a),$$
$$t_{3r} = 0, \quad t_{3\theta} = 0, \quad t_{33} = 0 \quad (x_3 = -h, \quad 0 \le r < \infty), \tag{1.26}$$

where t is the asymmetric Kirchhoff stress tensor, and the signs "+" and "–" refer to the upper and lower crack faces, respectively.

1.2.2. Governing Equations. The boundary-value problem posed can be reduced (after awkward transformations) to a homogeneous system of integral Fredholm equations of the second kind (the mathematics is detailed in [72]). If the roots of the characteristic equation are unequal, then this system has the following dimensionless form:

$$\frac{1}{2}\left(s\frac{k}{k_1} - q\right) f_1(\xi) + \frac{1}{2}\left(s\frac{k}{k_1} + q\right) f_2(\xi) + \frac{2}{\pi}\int_0^1 f_1(\eta) K_{11}(\xi,\eta)\,d\eta + \frac{2}{\pi}\int_0^1 f_2(\eta) K_{12}(\xi,\eta)\,d\eta + \frac{2}{\pi}\int_0^1 f_3(\eta) K_{13}(\xi,\eta)\,d\eta = 0,$$

$$\frac{1}{2}\left(s\frac{k}{k_1} + q\right) f_1(\xi) + \frac{1}{2}\left(s\frac{k}{k_1} - q\right) f_2(\xi) + \frac{2}{\pi}\int_0^1 f_1(\eta) K_{21}(\xi,\eta)\,d\eta + \frac{2}{\pi}\int_0^1 f_2(\eta) K_{22}(\xi,\eta)\,d\eta + \frac{2}{\pi}\int_0^1 f_3(\eta) K_{23}(\xi,\eta)\,d\eta = 0,$$

$$\frac{1}{2} s\frac{k}{k_2} f_3(\xi) + \frac{2}{\pi}\int_0^1 f_1(\eta) K_{31}(\xi,\eta)\,d\eta + \frac{2}{\pi}\int_0^1 f_2(\eta) K_{32}(\xi,\eta)\,d\eta + \frac{2}{\pi}\int_0^1 f_3(\eta) K_3(\xi,\eta)\,d\eta = 0. \tag{1.27}$$

The kernel of the integral equations is

$$K_{11}(\xi,\eta) = \xi^{n-1} n \left\{ \frac{s}{k}\left[\frac{k_2}{k_1}(k_1 + k_2) b_{n1} (\eta^{-n-1} S_n(z_{11}) - S_n(z_{21})) + (k_1 + k_2) b_{n2} (\eta^{-n-1} S_n(z_{12}) - S_n(z_{22})) \right.\right.$$
$$\left.\left. - 2k_2 (b_{n1} + b_{n2})(\eta^{-n-1} S_n(z_1) - S_n(z_2)) \right] - q b_{n3} (\eta^{-n-1} S_n(z_{13}) - S_n(z_{23})) \right\} + \xi^{2n} \sqrt{\pi}\, \frac{\Gamma(n+1)}{\Gamma(n+1/2)}$$
$$\times \left\{ \frac{s}{k}\left[\frac{k_2}{k_1}(k_1 + k_2)(R_n(b_{n1}, \eta) - R_n(b_{n1}, 1)) + (k_1 + k_2)(R_n(b_{n2}, \eta) - R_n(b_{n2}, 1)) \right.\right.$$
$$\left.\left. - 4k_2 \left(R_n\left(\frac{b_{n1} + b_{n2}}{2}, \eta \right) - R_n\left(\frac{b_{n1} + b_{n2}}{2}, 1 \right) \right) \right] - q(R_n(b_{n3}, \eta) - R_n(b_{n3}, 1)) \right\}, \ldots, \tag{1.28}$$

where

$$S_n(z) = \frac{1}{4}(z^2 - 1)^{-1} [Q_n(z) - z Q_{n-1}(z)], \qquad R_n(b,t) = \frac{1}{2} b (b^2 + t^2)^{-n-1},$$

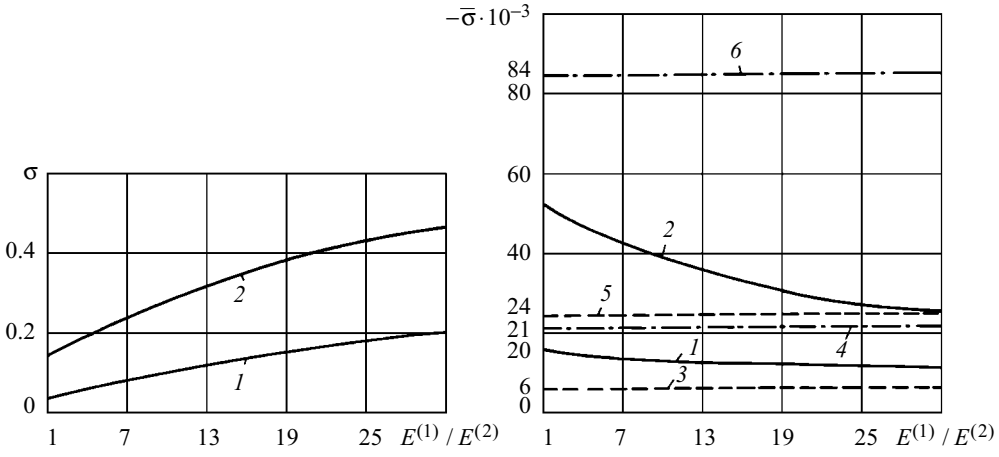

a b

Fig. 1

$$z_{11}=\frac{b_{n1}^2+\eta^2+\xi^2}{2\eta\xi},\qquad z_{12}=\frac{b_{n2}^2+\eta^2+\xi^2}{2\eta\xi},\qquad z_{13}=\frac{b_{n3}^2+\eta^2+\xi^2}{2\eta\xi},$$

$$z_{21}=\frac{b_{n1}^2+1+\xi^2}{2\xi},\qquad z_{22}=\frac{b_{n2}^2+1+\xi^2}{2\xi},\qquad z_{23}=\frac{b_{n3}^2+1+\xi^2}{2\xi},$$

$$z_1=\frac{\frac{1}{4}(b_{n1}+b_{n2})^2+\eta^2+\xi^2}{2\eta\xi},\qquad z_2=\frac{\frac{1}{4}(b_{n1}+b_{n2})^2+1+\xi^2}{2\xi},$$

$$b_{ni}=2\beta_i,\qquad \beta_i=n_i^{-1/2}ha^{-1}\qquad (i=\overline{1,3}). \tag{1.29}$$

Here $\Gamma(x)$ is the gamma function and $Q_n(z)$ are Legendre functions of the second kind.

Since the data obtained in [3–5, 22, 24–27, 62–66, 69, 80, 93] for near-surface cracks in hyperelastic, composite, and elastoplastic materials are very extensive and have already been covered in detail in [24, 25] and the scope of the present publication is limited, we will restrict ourselves to spatial axisymmetric problems for composites as the most interesting, in our opinion, case.

From the extensive studies on composite materials it follows that the buckling of a composite compressed along delamination (which corresponds to study into the possibility of subcritical fracture) is the initial stage of fracture after which other fracture mechanisms may be actuated.

1.2.3. Approximate Design Model. Fracture of composites with delaminations is an important issue. It was intensively studied by domestic and foreign scientists. Two stages of the fracture process are distinguished: initial stage, characterized by local buckling near cracks, and postcritical (after buckling) development of the defect. The first stage is treated within the framework of the approximate approach in the overwhelming majority of cases. Thus, an approximate design model for a disk-shaped delamination of radius a located at a distance h to the free surface of the composite consists in determining the Euler critical compressive stress σ_{11}^0 for a circular plate of radius a and thickness h compressed by uniform forces of intensity σ_{11}^0 per unit area of the lateral surface of the plate. The plate is as a rule assumed to be rigidly restrained. The simple-support conditions are also an option. Since the critical compressive stresses for rigidly restrained and simply supported plates differ substantially, we must admit that the initial stage of fracture of composites compressed along delaminations has been studied inadequately within the framework of the approximate approach. It is also obvious that the approximate approach is a fortiori inapplicable for large values of $\beta\equiv h/a$.

In the notation adopted, the Euler critical stress is described by the formula

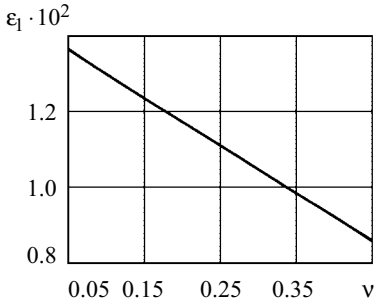

Fig. 2

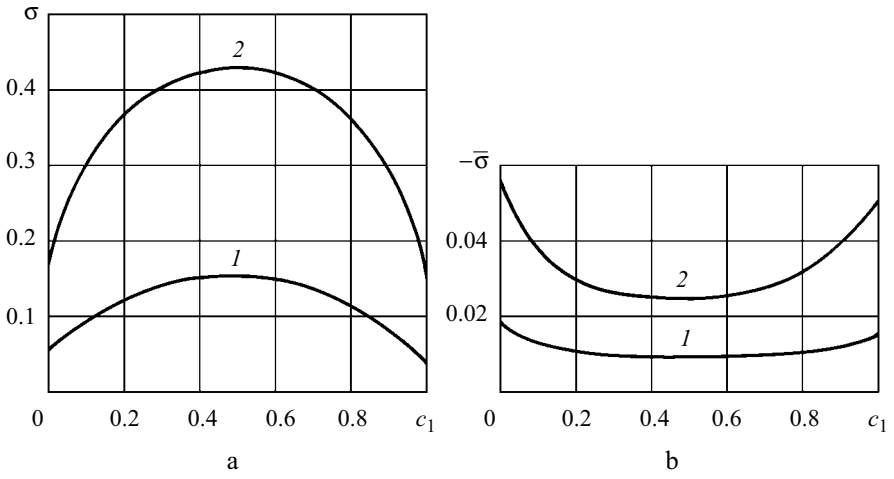

Fig. 3

$$-(\sigma_{11}^0)_{Eu} = \alpha \frac{\beta^2 E}{12(1-\nu^2)}, \tag{1.30}$$

where E is the reduced elastic modulus in the plane of isotropy (the plane of defect) and ν is Poisson's ratio. The coefficient α depends on the boundary conditions for the plate: $\alpha = 14.68$ (rigid restraint) and $\alpha = 4.196$ (simple support). Thus, the Euler critical stresses for rigidly restrained and simply supported plates differ by a factor of 3.5.

Note that cracks in composites are considered to be much larger than structural elements of the material, i.e., macrocracks are considered. Fracture processes in which piecewise-homogeneous properties are manifested (interfacial fracture, etc.) are not investigated, and the composite is modeled by an anisotropic medium with reduced characteristics. For the state of the art of studying interfacial fracture based on the approximate approach see [13].

1.2.4. Some Results. Let us discuss some results for near-surface disk-shaped delaminations in composites with reduced characteristics of a transversely isotropic medium (spatial axisymmetric case).

Laminated Composite with Isotropic Layers. At macrolevel, it is a transversely isotropic medium. The macrodelamination is in the plane of isotropy (parallel to the inner interfaces and the free surface of the composite).

Figure 1a, b shows the dimensionless critical stresses σ and $\bar{\sigma}$ (compressive stresses divided by the critical compressive stress σ_{11}^{0*} for a noninteracting crack and by the reduced elastic modulus E in the plane of isotropy) as functions of the ratio of elastic moduli $E^{(1)} / E^{(2)}$ of isotropic layers with equal Poisson's ratios. Curves *1* correspond to $\beta = ha^{-1} = 1/8$ and curves *2* to $\beta = 1/4$. As the ratio $E^{(1)} / E^{(2)}$ increases, the critical stress σ ($\bar{\sigma}$) monotonically increases (decreases). In contrast to a free crack, the critical compressive stresses decrease by more than an order of magnitude over the range of β involved.

For comparison, Fig. 1b shows the dimensionless Euler stresses $(\sigma_{11}^0)_{Eu} / E$ for simple-support conditions (dashed curves) and for rigid-restraint conditions (dash-and-dot curves) for $\beta = 1/8$ (curves *3* and *4*) and $\beta = 1/4$ (curves *5* and *6*).

Figure 2 shows the critical compressive strain $\varepsilon_1 = 1 - \lambda_1$ as a function of ν for a laminated composite with $\nu^{(1)} = \nu^{(2)} = \nu$, $E^{(1)} / E^{(2)} = 3$, and $c_1 = 0.3$ of the layer with $E^{(1)}$ ($\beta = ha^{-1} = 1/8$).

Figure 3a, b shows σ and $\bar{\sigma}$ as functions of the concentration c_1 of glass in a glass-based laminated composite (aluminoborosilicate glass plus epoxy maleic resin). Curves *1* and *2* correspond to $\beta = 1/8$ and $\beta = 1/4$, respectively. As can be seen from the figures, the critical compressive stresses are strongly dependent on the concentration of the composite components.

Composite Randomly Reinforced in the Planes y_3 = const with Short Ellipsoidal Fibers. At macrolevel, it is a transversely isotropic medium with y_3 = const as the plane of isotropy.

Figure 4 shows the dependences $\varepsilon_1 = \varepsilon_1(\beta)$ and $\bar{\sigma} = \bar{\sigma}(\beta)$ for a carbon-fiber-reinforced plastic with fiber concentration c_1 = 0.7 and fiber aspect ratio equal to 10. As $\beta \to \infty$, ε_1 and $\bar{\sigma}$ asymptotically tend to the critical values 0.085 and –0.097, respectively, for a free isolated delamination. When $\beta \geq 4$, the critical compressive stress is less than 5% different from that for an

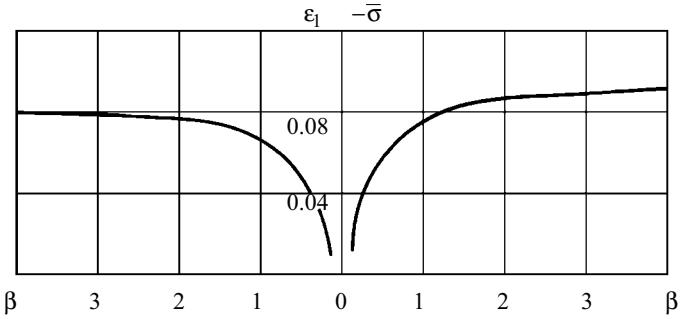

Fig. 4

isolated delamination. Approximate design models predict the dimensionless Euler critical stress $(\sigma_{11}^0)_{Eu} / E$ with a large error even for relatively small values of β (for example, $(\sigma_{11}^0)_{Eu} / E = -0.078$ when $\bar{\sigma} = -0.032$ for rigid-restraint conditions, i.e., these values differ by a factor of 2.5).

1.3. Interacting Internal Cracks.

1.3.1. Two Parallel Internal Cracks. Two interacting internal parallel cracks were studied in [16–19, 30, 59, 75, 92, 94]. Let us consider, as an example, the formulation of the spatial axisymmetric problem (1.5) [92].

Let an infinite material contain two internal coaxial disk-shaped cracks of radius a in the planes $y_3 = 0$ and $y_3 = -2h$ (y_j are the coordinates of the initial strain state). The boundary conditions of the linearized problem are

$$\widetilde{Q}_{33} = 0, \quad \widetilde{Q}_{3r} = 0 \quad (y_3 = (0)_{\pm}, 0 \le r \le a),$$

$$\widetilde{Q}_{33} = 0, \quad \widetilde{Q}_{3r} = 0 \quad (y_3 = (-2h)_{\pm}, 0 \le r \le a), \tag{1.31}$$

where $\widetilde{Q}_{ij}$ are the components of the asymmetrical stress perturbation tensor divided by the area in the initial strain state, (r, θ, y_3) is a cylindrical coordinate system, and the subscripts "$\pm$" refer to the corresponding crack faces.

Owing to mechanical and geometrical symmetry, the stress and strain fields can be represented as the sum of symmetric and asymmetric (about the plane of symmetry $y_3 = -h$) parts. And owing to linearity, these parts can be treated separately, as the symmetric and flexural buckling modes. Since these modes are symmetric, we can consider the upper half-space $y_3 \ge -h$ with the corresponding boundary conditions

$$\widetilde{Q}_{33} = 0, \quad \widetilde{Q}_{3r} = 0 \quad (y_3 = (0)_{\pm}, 0 \le r \le a),$$

$$\widetilde{Q}_{33} = 0, \quad u_r = 0 \quad (y_3 = -h, 0 \le r \le \infty) \tag{1.32}$$

for the flexural mode and

$$\widetilde{Q}_{33} = 0, \quad \widetilde{Q}_{3r} = 0 \quad (y_3 = (0)_{\pm}, 0 \le r \le a),$$

$$\widetilde{Q}_{3r} = 0, \quad u_3 = 0 \quad (y_3 = -h, 0 \le r \le \infty) \tag{1.33}$$

for the symmetric mode.

After some transformations, the boundary-value problems (1.32) and (1.33) reduce to a system of two integral Fredholm equations of the second kind with an additional condition for an unknown constant. For the flexural mode, this system has the following dimensionless form:

$$f(\xi) - \frac{1}{\pi k}\int_0^1 M_1(\xi, \eta) f(\eta) d\eta - \frac{1}{\pi k}\int_0^1 N_1(\xi, \eta) g(\eta) d\eta = 0,$$

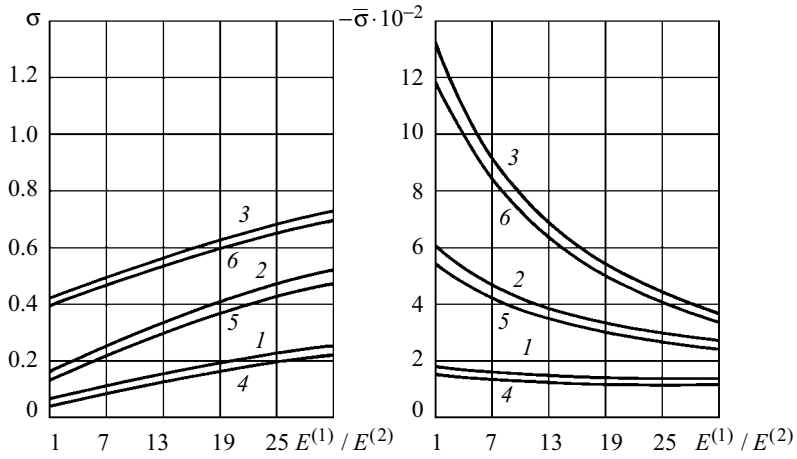

a b

Fig. 5

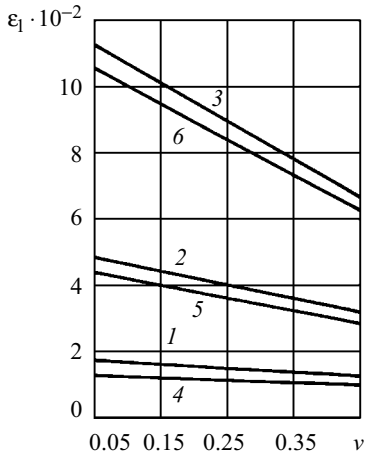

Fig. 6

$$g(\xi)-\frac{1}{\pi k}\int_0^1 M_2(\xi,\eta)g(\eta)d\eta-\frac{1}{\pi k}\int_0^1 N_2(\xi,\eta)f(\eta)d\eta=\text{const},$$

$$0\le\xi\le 1,\quad 0\le\eta\le 1, \tag{1.34}$$

where "const" is an unknown constant determined from the additional condition

$$\int_0^1 g(\xi)d\xi=0. \tag{1.35}$$

The kernels of the equations are defined by

$$M_1(\xi,\eta)=R_1(\eta+\xi)+R_1(\eta-\xi)-R_1(1+\xi)-R_1(1-\xi),$$

$$R_1(\zeta)=2\beta_1 k_2(4\beta_1^2+\zeta^2)^{-1}-2\beta_2 k_1(4\beta_2^2+\zeta^2)^{-1},$$

$$\beta_i=n_i^{-1/2}ha^{-1},\quad \text{etc.} \tag{1.36}$$

Let us cite some results for two coaxial disk-shaped delaminations (spatial axisymmetric case). These will be the critical compressive stresses of the flexural buckling mode as those that are much greater than the critical stresses of the flexural mode (in other words, it is the flexural buckling mode that is realized).

Laminated Composite with Isotropic Layers. At macrolevel, it is a transversely isotropic medium. Figures 5–7 show σ, $\overline{\sigma}$, and ε_1 (see the notation in the previous section) as functions of the stiffness characteristics and the concentration of composite components. Curves *1*, *2*, and *3* correspond to internal delaminations with $\beta=ha^{-1}$ ($2h$ is the distance between delaminations and a is their radius) equal to 1/16, 1/8, and 1/4, respectively. For comparison, the figures also include curves *4*, *5*, and *6* for a near-surface delamination, for two internal delaminations with the same distance between them as in the first case, and for a delamination at the same distance from the free surface as in the second case.

Figure 5a, b shows σ and $\overline{\sigma}$ as functions of $E^{(1)}/E^{(2)}\ge 1$ for a composite with $\nu^{(1)}=\nu^{(2)}=0.3$ and concentration c_1 of the layer with $E^{(1)}$.

Figure 6 shows the dependences $\varepsilon_1=\varepsilon_1(\nu)$ for a composite with $\nu^{(1)}=\nu^{(2)}=\nu$, $E^{(1)}/E^{(2)}=0.3$, and $c_1=0.3$.

Figure 7a, b shows σ and $\overline{\sigma}$ as functions of the concentration c_1 of glass in a composition of aluminoborosilicate glass and epoxy maleic resin.

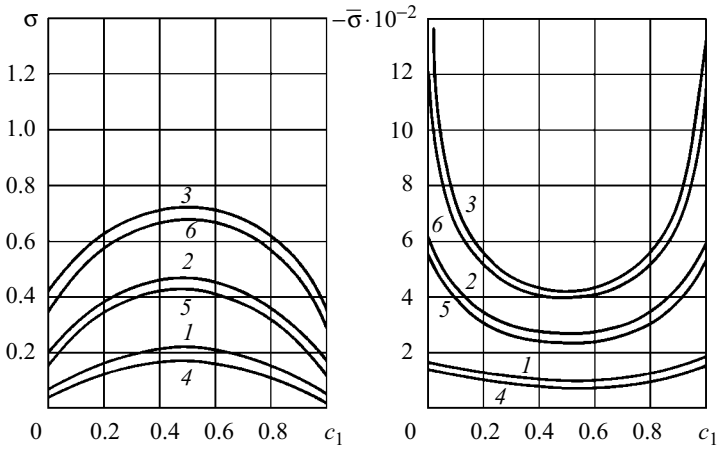

a b

Fig. 7

1.3.2. Periodic Series of Internal Parallel Cracks. Periodic interacting parallel cracks were studied in [23, 28, 29, 68]. Let us discuss, as an example, the formulation of the plane problem (1.1) [28].

Consider an infinite row of parallel equidistant cracks of equal length

$$\{x_2 = (2hn),\ |x_1| < a, -\infty < x_3 < +\infty\}, \quad n = 0, \pm 1, \pm 2, \ldots . \tag{1.37}$$

The material is compressed along the Ox_1-axis in parallel to the crack planes. The cracks are infinite along the Ox_3-axis. The crack faces are free from stresses. The boundary conditions of the linearized problem are

$$t_{22} = 0, \quad t_{21} = 0 \qquad (x_2 = (2hn)_{\pm},\ |x_1| < a,\ \ n = 0, \pm 1, \pm 2, \ldots), \tag{1.38}$$

where "+" and "–" refer to the crack faces. Considering the periodicity and symmetry (antisymmetry) of the stress and strain fields, we obtain the following boundary conditions for the layer $\{0 \le |x_1| < \infty, 0 \le x_2 \le h, 0 \le |x_3| < \infty\}$:

$$u_1 = 0 \quad (x_2 = 0,\ |x_1| > a), \quad t_{21} = 0 \quad (x_2 = 0,\ |x_1| < a),$$

$$t_{22} = 0 \quad (x_2 = 0, 0 \le |x_1| < \infty), \quad u_1 = 0 \quad (x_2 = h, 0 \le |x_1| < \infty), \quad t_{22} = 0 \quad (x_2 = h, 0 \le |x_1| < \infty) \tag{1.39}$$

for the flexural mode and

$$u_2 = 0 \quad (x_2 = 0,\ |x_1| > a), \quad t_{22} = 0 \quad (x_2 = 0,\ |x_1| < a),$$

$$t_{21} = 0 \quad (x_2 = 0, 0 \le |x_1| < \infty), \quad u_2 = 0 \quad (x_2 = h, 0 \le |x_1| < \infty), \quad t_{21} = 0 \quad (x_2 = h, 0 \le |x_1| < \infty) \tag{1.40}$$

for the symmetric mode.

The solution for the whole infinite plane can be obtained by extending the solutions of problems (1.39) and (1.40) for the layer $0 \le x_2 \le h$ to the domain $|x_2| \le h$ and then applying the periodicity conditions.

Finally, after a series of transformations, the boundary-value problems (1.39) and (1.40) reduce to the following eigenvalue problem (with respect to λ_1 or σ_{11}^0) for the homogeneous integral Fredholm equation of the first kind:

$$\int_0^1 f(\eta) \ln \left| \frac{1-\xi^2}{\eta^2 - \xi^2} \right| d\eta - \int_0^1 f(\eta) M(\xi, \eta) d\eta = 0, \quad 0 \le \xi < 1, \quad 0 \le \eta \le 1,$$

$$M(\xi, \eta) = R(\eta + \xi) + R(\eta - \xi) - R(1 + \xi) - R(1 - \xi), \tag{1.41}$$

where

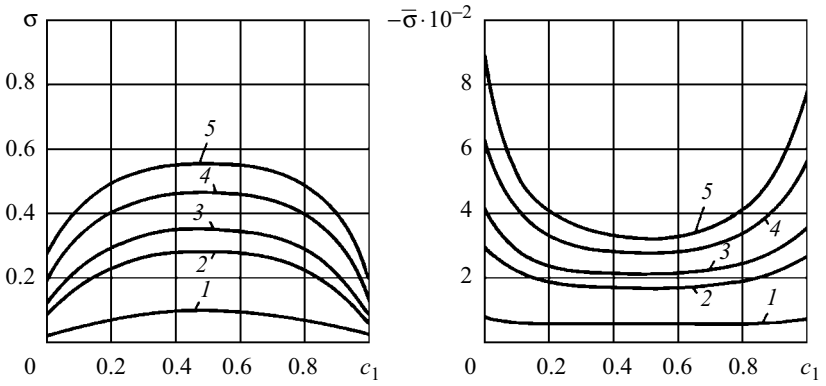

a b

Fig. 8

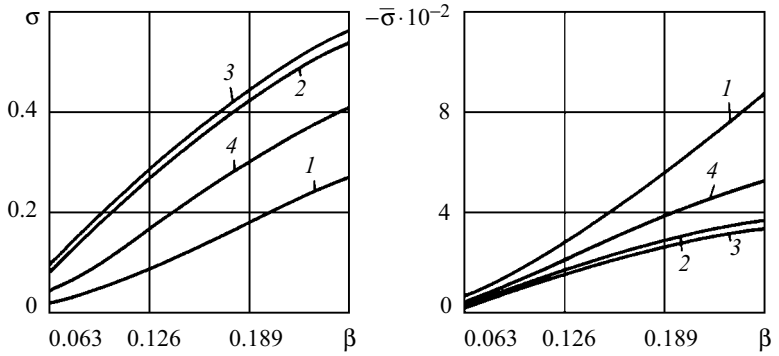

a b

Fig. 9

$$R(\zeta)=(-1)^{\alpha}\frac{\zeta\pi}{2\beta_1 k}\coth\frac{\zeta\pi}{2\beta_1}-2\,\mathrm{Re}\ln\Gamma\left(1+i\frac{\zeta}{2\beta_1}\right) \tag{1.42}$$

in the case of equal roots and

$$R(\zeta)=\frac{2}{k}\left[k_2\,\mathrm{Re}\ln\Gamma\left(1+i\frac{\zeta}{2\beta_\alpha}\right)\right]-k_1\,\mathrm{Re}\ln\Gamma\left(1+i\frac{\zeta}{2\beta_\gamma}\right) \tag{1.43}$$

in the case of unequal roots. Here $\beta_j=n_j^{-1/2}\beta$, $j=1,2;\ \beta=h/a;\ \alpha=2,\ \gamma=1$ for the symmetric buckling mode, and $\alpha=1,\gamma=2$ for the flexural mode.

Laminated Composite with Isotropic Layers: A Composition of Aluminoborosilicate Glass and Epoxy Maleic Resin. At macrolevel, it is a transversely isotropic medium. The composite has disk-shaped coaxial delaminations of radius a equally spaced at $2h$ and located in the planes of isotropy parallel to the interfaces. Let us discuss the results for the spatial axisymmetric case and the flexural buckling mode.

Figure 8a, b shows the dimensionless critical compressive stresses σ and $\bar{\sigma}$ as functions of the glass concentration c_1. Curves *1*, *2*, *3*, *4*, and *5* correspond to $\beta=h/a$ equal to 0.0625, 0.125, 0.15, 0.20, and 0.25, respectively.

Figure 9a, b shows σ and $\bar{\sigma}$ as functions of β for c_1 equal to 0, 0.3, 0.6, and 0.9 (curves *1*, *2*, *3*, and *4*).

Figure 10 compares the dependences of $\bar{\sigma}$ on c_1 for periodic delaminations, for two internal parallel delaminations, and for a near-surface macrocrack. Also Fig. 10 shows the dimensionless Euler critical stress $(\sigma_{11}^0)_{Eu}/E$ obtained by approximate design models (rigidly restrained and simply supported plate) for rather small relative distances between cracks: $\beta=1/16$ and $\beta=1/8$. The relative distances between delaminations (periodic series of delaminations, two parallel delaminations) or between a

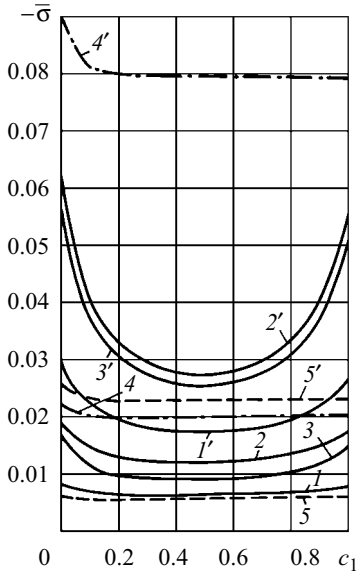

Fig. 10

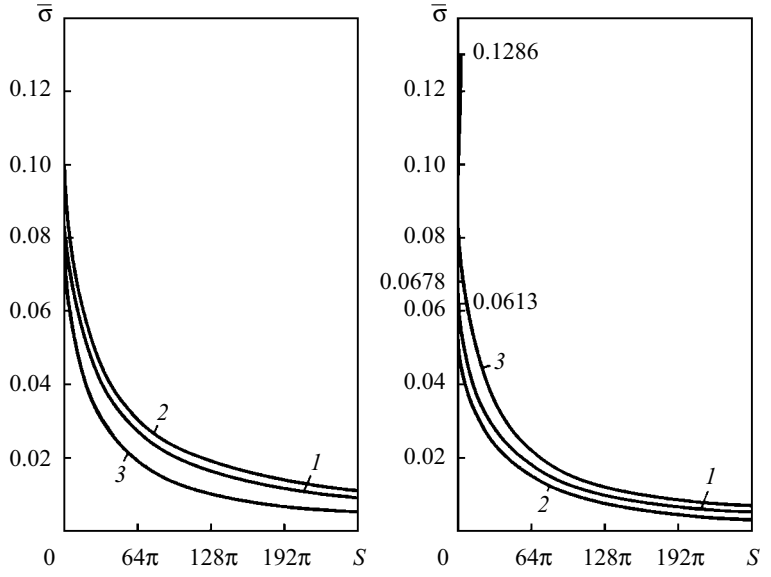

a b

Fig. 11

crack and the free surface of the material (near-surface delamination) are equal. Curves *1*, *2*, and *3* correspond to periodic delaminations, two parallel delaminations, and a near-surface delamination, respectively. Curves *4* and *5* represent the Euler critical stress for rigid-restraint and simple-support conditions, respectively. The curves with primed numbers refer to $\beta = 1/8$ and the other curves to $\beta = 1/16$.

Figure 11a, b shows σ and $\bar{\sigma}$ as functions of the dimensionless area $S = \pi a^2 / h^2$ of a defect in a periodic series of defects for the glass concentration c_1 equal to 0.3, 0.6, and 0.9 (curves *1*, *2*, and *3*, respectively). Specifying a value of σ or $\bar{\sigma}$, we can determine from these dependences what minimum area a delamination should have to grow further.

2. Theoretical Stability Analysis of Cracked Plates and Shells.

2.1. Formulation of Stability Problem of a Plate with a Crack. Consider an infinite thin isotropic elastic plate of thickness h weakened by a central through rectilinear crack of length $2l_0$ (Fig. 12) [15, 21, 72, 74]. At infinity, the plate is subjected to uniform forces of intensity p normal to the crack line. The stress p_y is always tensile, and the stress p_x is either tensile or compressive. The domain of the upper half plate where the stress p_x is compressive is hatched in Fig. 12. If the crack length is greater than the plate thickness, then the intensive compressive stresses acting along the crack periphery may cause local buckling of the plate prior to its fracture.

Local buckling near a central crack is analyzed using the static method within the framework of the von Karman linearized theory of plates. The governing equation and the boundary conditions at the crack periphery free from external forces are

$$|\omega'|^{-6}\,[L - \lambda\tilde{L}]\,W = 0, \qquad \lambda = \frac{6pl_0^2(1-\nu^2)}{Eh^2}, \qquad |\omega'|^{-4}\,MW|_{\rho=1} = 0,$$

$$|\omega'|^{-5}\,\tilde{Q}W\big|_{\rho=1} = 0, \qquad W|_{\rho\to\infty} \to 0, \tag{2.1}$$

where $L, \tilde{L}, M$, and $\tilde{Q}$ are differential operators; $\omega(\zeta)$ is a function conformally mapping the exterior of the crack onto the exterior of a unit circle; and ν and E are the elastic constants.

Since buckling is local, the deflection W must subside to infinity:

$$W|_{\rho\to\infty} \to 0. \tag{2.2}$$

The eigenvalues of the problem depend on Poisson's ratio alone and do not depend on the geometrical parameters h and $2l_0$. Denote the minimum positive eigenvalue by λ_*. Then the critical stress p_{cr} causing local buckling is defined by

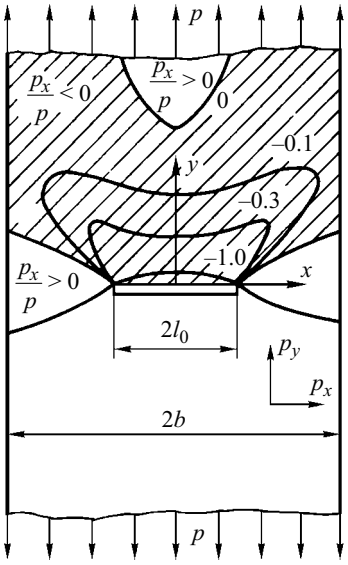

Fig. 12

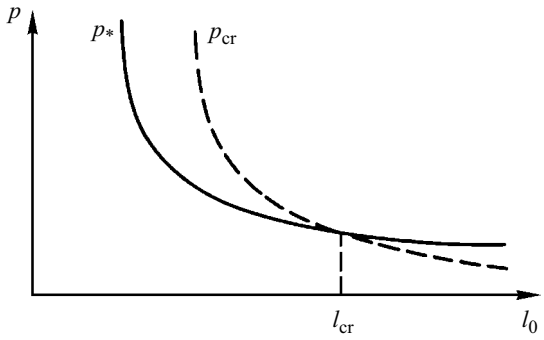

Fig. 13

$$p_{\rm cr} = \frac{\lambda_*(\nu)\,E}{6(1-\nu^2)}\left(\frac{h}{l_0}\right)^2. \tag{2.3}$$

If the crack length is larger than some critical value denoted by l_*, then local buckling precedes fracture. We will determine l_* by comparing the critical stress $p_{\rm cr}$ (2.3) and the fracture stress p_* predicted by the Griffith–Irwin theory:

$$p_* = \sqrt{\frac{2E\gamma}{\pi h}}\left(\frac{h}{l_0}\right)^{1/2}, \tag{2.4}$$

where γ is the effective surface energy density of a brittle or quasibrittle material. Then we have

$$l_* = \left[\frac{\lambda_*^2(\nu)E\pi h^4}{72(1-\nu^2)\gamma}\right]^{1/3}. \tag{2.5}$$

Figure 13 shows the qualitative dependence of $p_{\rm cr}$ and p_* on l_0. As is seen, buckling precedes fracture when $l_0 \succ l_*$ and fracture precedes buckling when $l_0 \prec l_*$.

2.2. Eigenvalue Calculation. We will calculate the eigenvalues using the variational method that has been developed to solve stability problems for deformed thin bodies with cracks. The basic variational equation is:

$$\int_0^{2\pi}\int_1^{\infty} |\omega'|^{-4}\left(L-\lambda\widetilde{L}\right) W\delta W\rho\,d\rho\,d\theta + \int_0^{2\pi} |\omega'|^{-4}\,MW\frac{\partial\delta W}{\partial\rho}\bigg|_{\rho=1} d\theta + \int_0^{2\pi} |\omega'|^{-4}\,\widetilde{Q}W\delta W|_{\rho=1}\,d\theta = 0. \tag{2.6}$$

The system of coordinate functions is selected in the form

$$W = |\omega'|^4 \sum_{m=0}^{M}\sum_{n=1}^{N} A_{nm}\,\rho^{-n}\cos m\theta. \tag{2.7}$$

The characteristic equation derived from the linear system of homogeneous algebraic equations has been solved numerically on a computer for different numbers of coordinate functions Ω and for $\nu = 0.3$. The computed results are summarized in Table 4.

Introducing the notation

TABLE 4

N	2	4	6	8
Ω	4	12	24	40
λ_*	25	5.945	5.516	5.508

TABLE 5

η	8	4	2	1	0.5	0	–0.5	–1	–2	–4	–8
λ_*	69.79	38.47	20.26	14.78	8.64	5.51	3.69	2.87	1.98	1.21	0.84

$$K = \frac{\lambda_{(\alpha)}(\nu)}{6(1-\nu^2)}, \tag{2.8}$$

we transform (2.3) into the form

$$p_{\rm cr} = KE\left(\frac{h}{l_0}\right)^2, \tag{2.9}$$

whence if $\lambda_* = 5.516$, then $K = 1.01$.

The problem of finding the minimum positive eigenvalue was solved in an exact formulation using the collocation method [72, 74]. According to this method, the coordinates of the points called collocation points at which the equilibrium equation and boundary conditions are satisfied are substituted into theses equations. These points are selected so as to provide satisfactory convergence of the solution. The resulting value of K is in good agreement with that produced by the variational method.

2.3. Stability of Plates with Cracks and Crack-Like Defects under Various Loading Conditions. The approach developed in [72, 74, 78] for stability analysis of thin cracked bodies was used to study the local buckling of plates with various crack-like defects under various loading conditions.

For plates with a circular or noncircular hole, the critical stress is defined [20, 77] by

$$p_{\rm cr} = \frac{\lambda_*(\nu,\varepsilon)E}{24(1-\nu^2)}\left(\frac{h}{R}\right)^2, \tag{2.10}$$

where $R = (a+b)/2$ and $\varepsilon = (a-b)/(a+b)$ are the geometrical characteristics of the hole, a and b are the major and minor semiaxes of ellipse.

For a plate with an arbitrarily oriented rectilinear crack [72, 74], the critical load is defined by

$$p_{{\rm cr}(\alpha)} = \frac{E\lambda_*(\nu,\alpha)}{6(1-\nu^2)}\left(\frac{h}{l_0}\right)^2, \qquad K_{(\alpha)} = \frac{\lambda_*(\nu,\alpha)}{6(1-\nu^2)}, \tag{2.11}$$

where α is the angle between the line of action of the tensile force and the crack line.

For a plate with a rectilinear crack under biaxial loading, the critical stress is defined [76] by

$$p_{\rm cr} = \frac{\lambda_*(\nu,\eta)E}{6(1-\nu^2)}\left(\frac{h}{l_0}\right)^2, \qquad \eta = \frac{q}{p}, \tag{2.12}$$

where q is the load acting along the crack.

TABLE 6

R, mm	$\eta_* \cdot 10^2$			
	l_0 = 10 mm	l_0 = 20 mm	l_0 = 30 mm	l_0 = 40 mm
4000	0.0596	0.0592	0.0594	0.0591
2000	0.119	0.121	0.118	—
1500	0.159	0.160	0.160	—
1000	0.239	0.237	—	—

Table 5 summarizes the minimum positive eigenvalues λ_* calculated for $\nu = 0.3$ and several values of η.

For a plate with a square hole under plane stress, the critical stress is defined [74] by

$$p_{\mathrm{cr}(\kappa)} = \frac{\lambda_*(\nu,\varepsilon)E}{24(1-\nu^2)}\left(\frac{h}{R}\right)^2, \qquad K_{(\kappa)} = \frac{\lambda_*(\nu,\varepsilon)}{24(1-\nu^2)}, \tag{2.13}$$

where R is the scale factor, and ε is the geometrical parameter of the hole, $0 \le \varepsilon \le 1$.

2.4. Stability of a Cylindrical Shell with a Crack. In studying the local buckling of a cylindrical shell with a crack under tension, it is necessary to take into account the transverse–longitudinal bending of the shell associated with its curvature. This is a very difficult mathematical task. Therefore, this problem has been solved by the collocation method [45, 72, 74].

Consider a shallow shell with a small crack under uniform tensile forces. The stability equations are

$$\frac{D}{h}\nabla^4 W = L(W,\varphi^0) + L(W^0,\varphi) - \nabla_k^2\varphi, \qquad \frac{1}{E}\nabla^4\varphi = -L(W^0,W) + \nabla_k^2 W, \tag{2.14}$$

where φ is the stress function, W is the deflection function of the median surface of the shell, and the superscript "0" refers to the subcritical stress state.

If cracks are small, then

$$\frac{l_0^2}{Rh} < 1. \tag{2.15}$$

Since the buckling problem is solved approximately, we set W^0 equal to zero and assume that φ^0 is the same as that of the plate. The perturbed state is damped at infinity, i.e.,

$$W\big|_{\sqrt{x^2+y^2}\to\infty} \to 0. \tag{2.16}$$

The critical stress is determined from the expression

$$p_{\mathrm{cr}} = \frac{\lambda_*(\nu,R,h,l_0)}{6(1-\nu^2)}\frac{Rh}{l_0^2}. \tag{2.17}$$

In contrast to the plate, here the eigenvalues also depend on the geometrical parameters: radius, thickness, and crack length. Table 6 summarizes values of λ_* calculated for $\nu = 0.3$ and $h = 0.44$ mm. The radius R of the shell and the half-length l_0 of the crack were selected from the condition (2.15). The number of coordinate functions was $\Omega = 24$.

3. Experimental Investigation of Stability and Fracture of Plates and Shells with Cracks. Here we analyze the influence of near-crack buckling of plates and shells on their fracture.

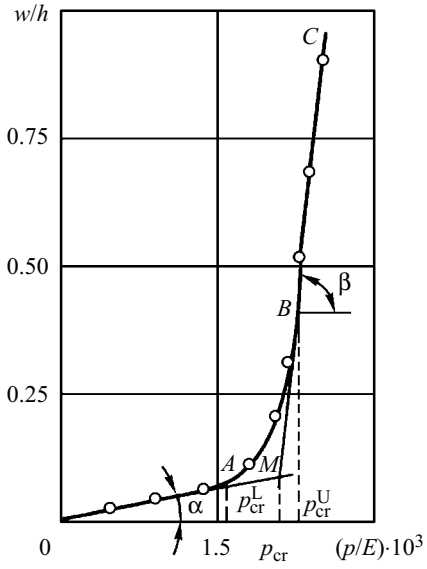

Fig. 14

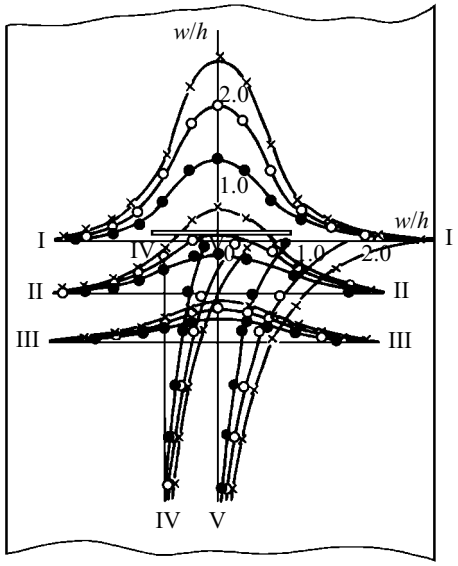

Fig. 15

3.1. Stability of Plates and Shells with Cracks.

3.1.1. Experimental Technique. The subjects of testing were rectangular plates made of various structural materials, such as aluminum and titanium alloys and steels, and containing fatigue cracks and slits. The plates were stretched via intermediate clamps on a TsD-10/90 testing machine. The deflections of the plates near cracks were measured with multipoint devices equipped with pneumatic displacement transducers [58, 72, 74]. The strain state was measured with KF-5 resistance strain gauges. The gauges were glued at characteristic sections of the plate, on two sides, strictly opposite to each other. This made it possible to measure the surface strains on two sides of the plate and use them to calculate the flexural strains and the strains of the median surface. The stresses were measured by the photoelastic method in plates made of optically active material ÉD-16M. In steel plates, the stresses near a crack or slit were determined from the measured strains using Hooke's law. Cylindrical panels and cylindrical and conic shells were tested in much the same way as the plates. To this end, special means of loading and strain measurement had been developed [38, 41, 74].

3.1.2. Buckling Stresses. The deflection W or strain difference $\Delta\varepsilon$ were adopted as buckling characteristics of plates, and the stress dependences of W or $\Delta\varepsilon$ was plotted [73, 78, 89]. Figure 14 shows such a dependence (deformation curve) for a plate made of D16T material. The thickness of the plate is h = 0.98 mm and the ratio of the crack half-length to the plate width is l_0 / b = 0.2. Three characteristic sections can be observed on the curve: OA, characterizing the initial equilibrium state of the plate; BC, characterizing the new equilibrium state; and AB, a transitive section. The critical stress p_{cr} was determined as the abscissa of the point M at which the continuations of the rectilinear sections OA and BC intersect and by the Southwell method [72, 74]. The stresses p_{cr} determined by the two methods differ insignificantly. The experimentally established dependence of p_{cr} on the geometrical and mechanical characteristics of the plate is

$$p_{cr} = KE\left(\frac{h}{l_0}\right)^2, \tag{3.1}$$

which fits well the theoretical dependence (2.9). This allows us to compare theoretical and experimental results.

When the mechanical and geometrical characteristics of the plate are known, it is sufficient to calculate the coefficient K to find p_{cr}. Table 7 collects values of K for some tested materials.

The effect of the following factors on the coefficient K was studied: small distance between the crack and the plate edge, large width of the crack, nonrectilinearity (curvature) of the crack; nonperpendicularity of the crack to the line of action of the load, and curvature of the plate surface. Empirical expressions for determining K depending on the geometrical parameters of plates and defects were derived in [81].

TABLE 7

Material	St. 08kp	St. 20	St. 65G	VT-1-1	AMg6M	D16T	AMtsM
h, mm	1.02	0.54	0.51	0.42	0.93	0.97	0.92
K	1.10	1.15	1.0	1.02	1.15	1.15	1.15

The effect of the plastic deformation of plates on the critical stresses was studied. It was established that the plasticity of the material not only near the crack periphery but also in the section running through the crack strongly decreases the coefficient K. The following empirical dependence was derived in [48] for determining the coefficient K:

$$K = \begin{cases} 0.0088\left(\dfrac{2l_0}{h}\right)^{0.98} & \text{for} \quad \dfrac{2l_0}{h} < 140, \\ 1.12 & \text{for} \quad \dfrac{2l_0}{h} > 140. \end{cases} \tag{3.2}$$

Since the plates begin to buckle immediately after application of a tensile force, we can judge the buckling mode before the stress achieves the critical level. The portions of the plate near the crack faces bulge in the same direction relative to the plate plane. The buckling mode has axial symmetry with the longitudinal axis of the plate as the axis of symmetry. The deflection W is maximum near the crack and quickly decreases toward its tip and with distance from it along the longitudinal axis of the plate. Figure 15 shows the distribution of W over characteristic sections of an AMg6M plate with $h = 0.93$ mm and $l_0/b = 0.32$. The full circles, open circles, and x's correspond to $p = 60$, 80, and 100 MPa [72, 74].

3.1.3. Stability of Plates with Cracks and Crack-Like Defects under Various Loading Conditions. The technique developed in [72, 74] was used to test plates with various stress concentrators. For AMg6M plates of thickness $h = 0.93$ mm with an inclined crack of length $2l_0 = 100$ mm, the value of $K_{(\alpha)}$ varied from 1.15 to 9.50, depending on the angle α between the crack and the line of action of the load. The dependence $K_{(\alpha)}$ on K (with α varying from $\pi/2$ to $\pi/12$) can be represented [61, 72] as

$$K_{(\alpha)} = \frac{K}{\sin^3 \alpha}. \tag{3.3}$$

AMg6M plates of dimensions 500×240×0.48 mm with two cracks of length $2l_0 = 30$ mm were tested in two cases: parallel cracks and in-line cracks. It has been established that the critical stresses practically do not depend on the distance between the parallel cracks and the buckling mode near each of the parallel cracks is symmetric. In the case of in-line cracks, p_{cr} is also independent of the distance between the cracks when this distance is large. As the inter-crack distance decreases, p_{cr} abruptly drops because the buckling mode becomes antisymmetric [37, 72].

The plates tested under biaxial loading were made of AMg6M material and had the form of a cross with overall dimensions 400×400 mm, dimensions of the test portion (100×100) mm, $h = (0.48, 0.19)$ mm, $2l_0 = (20 – 60)$ mm. The critical stresses were determined theoretically and experimentally by the technique from [35, 36, 76]. The following empirical formula for $K_{(q)}$ has been derived:

$$K_{(q)} = K\left(1 + \frac{q}{p_{cr}}\right), \tag{3.4}$$

where q is the load acting along the crack, and p_{cr} and K pertain to the case of uniaxial tension. Table 8 summarizes values of $K_{(q)}$ determined experimentally, numerically, and theoretically.

The above-mentioned technique was used to test plates with some other defects such as an elliptic hole [77], curved cracks [42], pointed holes with three cuspidal points [40], and two radial cracks reaching the periphery of a circular hole [72].

TABLE 8

h, mm	l/b	q, MPa	q / p_{cr}	$K^e(q)$	$K^n(q)$	$K^t(q)$
0.48	0.22	0.1	0.07	1.22	1.23	1.09
		0.3	0.20	1.34	1.38	1.26
		0.5	0.33	1.50	1.53	1.37
	0.51	0.1	0.35	1.56	1.55	1.43
		0.3	1.05	2.50	2.36	1.92
		0.5	1.75	3.80	3.17	2.30

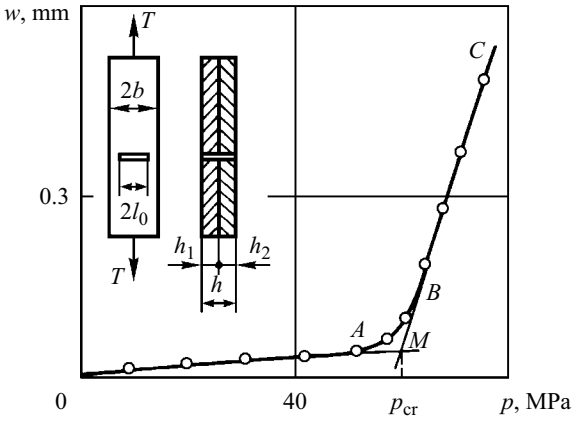

Fig. 16

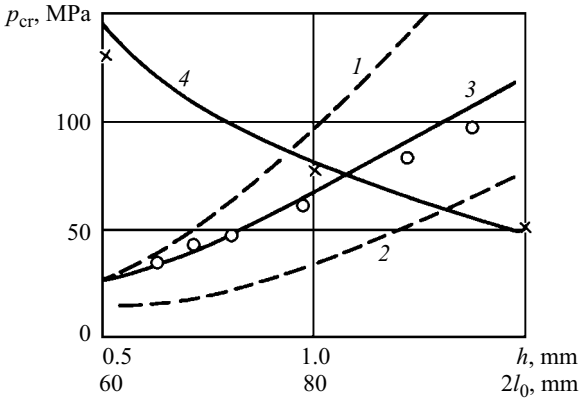

Fig. 17

The wide distribution of multilayer structural members (made of composites, metals with reinforcing and corrosion-resistant coatings, adhesive-bonded materials, etc.), which also may acquire cracks during manufacture and operation, necessitates studying near-crack buckling in such structures and its influence on the fracture characteristics. With this in mind, two-layer metal plates of total thickness h were tested. The layers of the plate are plates of thicknesses h_1 and h_2, one made of St. 20 steel and the other of AMg6M aluminum alloy, bonded together with BF-2 glue (Fig. 16) [51, 88]. The thickness h_1 was equal to 0.53 mm in all tests, and the thickness h_2 varied from 0.1 mm to 0.83 mm. The critical stress p_{cr} was determined from a deflection W versus stress p curve. Such a curve for a plate with $2b = 250$ mm, $2l_0 = 100$ mm, $h_1 = 0.53$ mm, and $h_2 = 0.45$ mm is shown in Fig. 16.

Let us determine the elastic modulus E for the two-layer plate by averaging the corresponding moduli of its components (E_1 for the steel and E_2 for the aluminum alloy) according to Voigt, assuming the uniformity of the generalized displacement field:

$$E = \psi_1 E_1 + \psi_2 E_2, \tag{3.5}$$

where ψ_1 and ψ_2 are the relative volume fractions of the components. Then considering the two-layer plate isotropic with an elastic modulus E, we can determine the critical stress p_{cr} from expression (3.1). The corresponding coefficient K is equal to 1.15, according to Table 7.

Figure 17 shows p_{cr} as a function of h for $2l_0 = 100$ mm (open circles) and as a function of $2l_0$ for $h_1 = 0.53$ mm and $h_2 = 0.3$ mm (x's). Curves *3* and *4* represent the theoretical stresses p_{cr} plotted from expression (3.5) for two-layer plates. Curves *1* and *2* also represent the theoretical critical stresses plotted from expression (3.1) for a single-layer steel plate ($E = E_1$) and aluminum plate ($E = E_2$), respectively, both of thickness h. As is seen, the experimental values of p_{cr} lie between curves *1* and *2*.

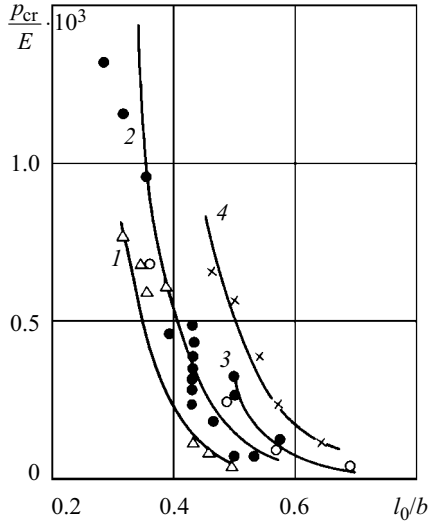

Fig. 18

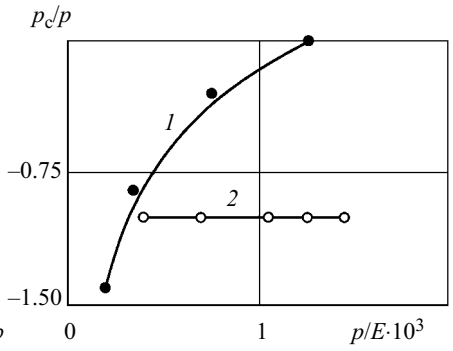

Fig. 19

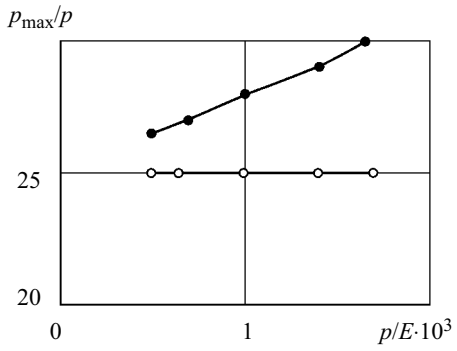

Fig. 20

Curve *3* fits these values well for relatively small values of h corresponding to small levels of p_{cr}. In turn, curve *4* describes well the experimental dependences of p_{cr} on $2l_0$ for relatively large values of $2l_0$, which also correspond to small values of p_{cr}.

Plates with an edge crack were tested in [14, 50, 52, 82, 84, 87]. Plates with an edge crack under tension deform differently from plates with a central crack. The main difference is in the mechanism of buckling, which is due to the way the load is applied. The load can be applied to plates in two ways: directly and through hinges. It is the latter case where local buckling may occur [14, 52, 87]. In this case the crack faces move apart, and the plate's portion near the edge opposite to the crack is subject to compression. The compressive stresses there may cause local buckling, depending on the geometry of the plate. It has been established that local buckling occurs when the ratio of the crack length l_0 to the plate width b is greater than 0.25. Figure 18 shows p_{cr} as a function of l_0/b for plates made of different materials. The symbols stand for the experimental data. Curves *1–4* have been plotted from an empirical formula for p_{cr} (curves *1* and *2* correspond to AMgbM plates of thicknesses $h = 0.28$ and 0.48 mm, respectively, curve *4* to an AMg2P plate of thickness $h = 0.95$ mm, and curve *3* has been plotted from the data [72] for 2024-T4 aluminum alloy). The following empirical formula for p_{cr} fits the experimental data best:

$$p_{cr} = KE\frac{h^2 b^4}{l_0^6}. \tag{3.6}$$

The following values of K have been obtained: $K = 0.2$ for AMg6M, $K = 0.18$ for AMg2P, and $K = 0.13$ for 2024-T4 [72].

3.1.4. Stress–Strain State of Plates with Cracks. Plates made of ÉD-16M material were subjected to two tests. One test allowed the plates to buckle. In the other test, two restraints were placed flat on two sides of the plate to prevent buckling and not to interfere with longitudinal deformation [54, 55, 72].

Figures 19 and 20 show the dependence of the compressive stresses p_c acting along the crack periphery and the tensile stresses p_{max} at the crack tip on the applied load. Curves *1* and *2* correspond to the cases of absence and presence of buckling. Also the figures show the dependence of the dimensionless deflection W/h at the middle of the crack face on the stress p. As is seen, p_c/p and p_{max}/p are independent of p in the absence of buckling. The normal deflection has a strong effect on the stress state near the crack. The ratio p_c/p increases, and for large p the median surface of the plate stretches. The ratio p_{max}/p increases with p, raising the stress concentration. For the given load, the buckling increases the stress concentration by approximately 19%.

The effect of buckling on the strain state of a St. 20 steel plate with $h = 0.5$ mm and $l_0/b = 0.13$ can be judged from Fig. 21. The figure shows the surface strains ε_{x_1} (curve *2*) and ε_{x_2} (curve *4*), flexural strains ε_{ux} (curve *1*), and the strains of the median surface ε_{ox} (curve *5*) as functions of p. Under small loads, the bending near cracks is absent or insignificant; therefore, the surface strains are negative on both sides of the plate. The degree of bending increases with p, making the strain ε_{x_1} on the convex side positive, the strain ε_{x_2} remaining negative. While the strain ε_{ux} is small, the strain ε_{ox} is compressive and increases

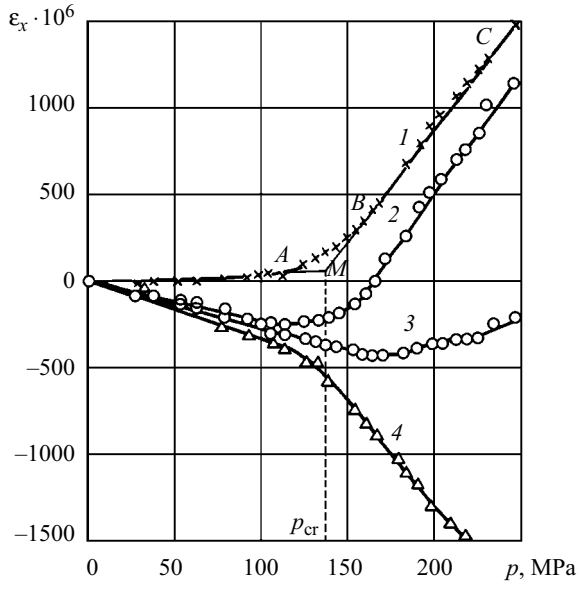

Fig. 21

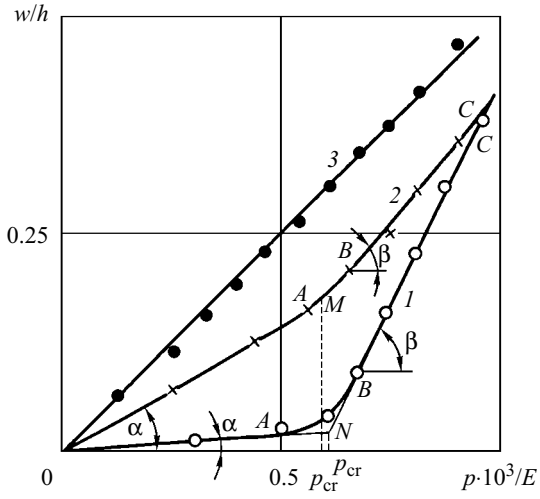

Fig. 22

TABLE 9

l_0, mm	R, mm				
	4000	2000	1500	1000	5000
40	0.77	0.73	0.72	0.67	0.64
30	0.77	0.76	0.75	0.67	0.66
25	0.78	0.76	0.75	0.70	0.68
20	0.88	0.78	0.78	0.77	0.72
15	0.88	0.86	0.80	0.80	0.78
10	0.90	0.87	0.82	0.80	0.80

in absolute magnitude with load. As ε_{ux} increases, the behavior of ε_{ox} changes: it starts decreasing, and at large buckling the median surface may become to be subject to tension rather than compression.

3.1.5. Stability of Shells with Cracks. Cylindrical panels and cylindrical and conic shells were tested in [38, 39, 41, 45, 57, 86]. Figure 22 shows deformation curves for panels with $2l_0$ = 30 mm and the following radii: R = 4000 mm (curve *1*), R = 1000 mm (curve *2*), and R = 250 mm (curve *3*). The deformation curves for panels of large radius are similar to the deformation curves for plates, which made it possible to determine p_{cr} and K using formula (3.1).

Table 9 summarizes the values of K obtained from tests on several panels differing in the radius and length of the crack. As R decreases, the deformation curve straightens, and K and p_{cr} cannot be determined. The diameter of the cylindrical shells was D = (70, 120, 180, 250) mm, $2l_0$ varied from 20 to 70 mm, and h = (0.30, 0.39, 0.46) mm. The tapering angle of the conic shells was φ = 40, 20°. The crack was circular with a diameter of 180 mm. The crack length varied from 20 to 60 mm. The deformation curves for all the shells are essentially different from those for plates and similar in form to those for a cylindrical

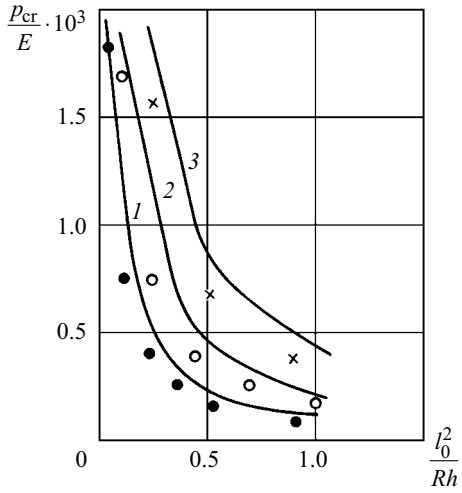

Fig. 23

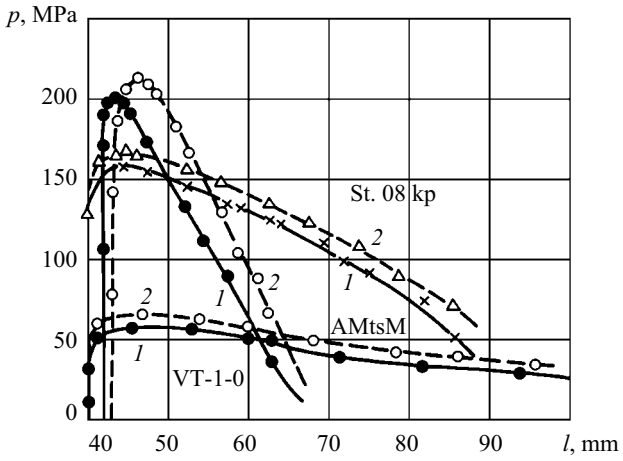

Fig. 24

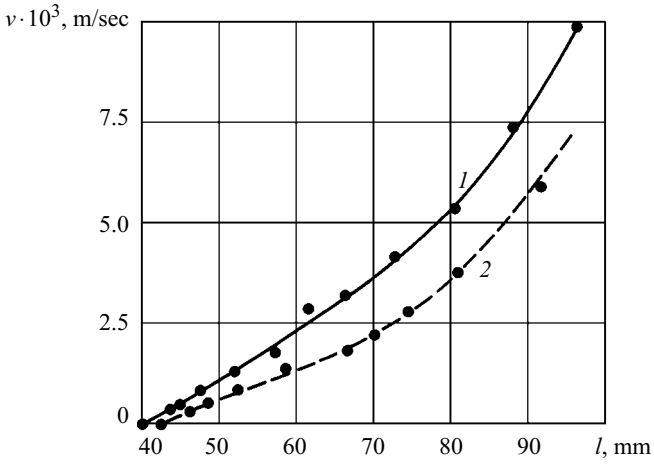

Fig. 25

panel of small radius. A typical feature of the curve is the linear dependence between the load and the deflection near the crack, which made it impossible to determine p_{cr} and K.

Figure 23 compares theoretical and experimental data for panels with $2b = 240$ mm and $h = 0.44$ mm. The experimental values of p_{cr} have been obtained with regard for the condition (2.15). The theoretical values (solid lines) of p_{cr} have been determined by formula (2.17) using the values of λ_* from Table 6. Curves *1–3* correspond to R = 4000, 2000, 1000 mm, respectively. As is seen, the experimental and theoretical results are in satisfactory agreement.

3.2. Fractures of Plates and Shells with Cracks.

3.2.1. Experimental Technique. A plate with a crack was loaded on a TSD-10/90 testing machine at a constant rate of $0.83\cdot 10^{-4}$ m/sec. Two cases were examined: with and without buckling. During fracture, the plate's portion near the crack and dynamometer scale was synchronously recorded with FOR-2 photorecorders. The chronophotographs were analyzed frame-by-frame with a toolmaker's microscope to determine the length of the growing crack, opening of its faces at fixed points, and the corresponding stresses [72–74]. In integrated crack-resistance testing of plates, the length of the growing crack was measured by the method of electric potential [72]. The displacements of the middle points of the crack faces and the points of load application were measured with strain-gauge displacement transducers. Then these data were used to determine and compare the fracture characteristics of plates with and without buckling.

3.2.2. Kinetics of Fracture of Plates. Figure 24 shows typical fracture curves for plates made of materials VT-1-0, AMtsM, and St. 08kp. Curves *1* and *2* correspond to the cases of buckling and no buckling. The form of the curves depends on the

TABLE 10

Material	$2b$, mm	h, mm	l_0, mm	ν_1, mm	ν_2, mm	δ
AMg6M	250	0.50	30.0	4.20	3.50	0.20
	250	0.50	41.5	2.20	1.85	0.19
	250	0.50	50.0	0.85	0.70	0.22
	250	1.02	42.0	1.40	1.12	0.25
	250	1.45	41.0	1.50	0.98	0.17
AMtsM	250	0.92	40.0	0.54	0.49	0.10
D16T	200	0.97	41.0	3.70	2.90	0.27
VT-1-0	160	1.01	42.5	0.17	0.15	0.13
Steel 20	250	0.52	42.0	0.47	0.41	0.14
Steel 08kp	200	1.03	40.0	0.43	0.37	0.16
Steel N36	250	0.43	39.5	3.40	2.60	0.31

material, dimensions, and shape of the plate and on whether buckling is present or absent. Analyzing the form of the curve, we can judge the influence of these factors on the fracture process and determine the following characteristics: the stress p_i at the beginning of crack growth, the maximum stress p_m, the crack half-length l_c at the beginning of avalanche-like fracture, the stress p_c at the beginning of avalanche-like fracture, and the crack growth rate v [72, 74].

Figure 25 shows the crack growth rate v as a function of the crack length l for AMg6M material (curves *1* and *2* correspond to the cases of buckling and no buckling, respectively). It is seen that at first v increases almost linearly and then abruptly. The crack growth rate v varies differently in plates made of different materials. For example, no abrupt change of v was observed until fracture of the VT-1-0 plates. An abrupt increase in the crack growth rate was detected at $l_c/b = 0.4$ in the N36 steel plates and at $l_c/b = 0.6$ in the AMg6M plates. The effect of buckling is such that a certain crack growth rate is achieved in buckled plates earlier than in plates with no buckling.

Table 10 collects the values of v for $l = 55$ mm for several materials (v_1 stands for the case of buckling and v_2 for the case of no buckling). The maximum value of v is observed for more elastic materials: D16T and N36. These values of v were used to establish the dependence of v on other fracture characteristics: time to fracture, crack length, and applied stress. Then these dependences were used to determine the values of l_c and p_c. It has been established that buckling decreases the stress p_i by 10–20% depending on the material of plates and decreases l_c and p_c by 5–10%.

3.2.3. Crack Resistance of Plates. Local buckling influences the crack-resistance characteristics of plates: mechanical (stress intensity factor K_I), deformation (crack tip opening displacement δ), and energy (J-integral) characteristics of elastoplastic fracture. It was studied using fracture curves: load p versus displacement s at the middle of crack faces and load p versus displacement s_p of points of load application [44]. Such curves for steel 20 plates with 170 mm width, $h = 0.77$ mm, and $2l_0 = 78$ mm are shown in Figs. 26 and 27. There are characteristic points marked: the point A corresponds to the moment of buckling, the point i to the moment of crack initiation, and the point c to the maximum load. As is seen, in case of buckling, the displacements s and s_p increase at a smaller load p, with p_i and p_c being smaller too.

The technique from [44] was used to determine characteristics of elastoplastic fracture for a number of materials. It has been established that such characteristics for plates with buckling preceding fracture are much less than those for plates with no buckling. The maximum difference is about 18%.

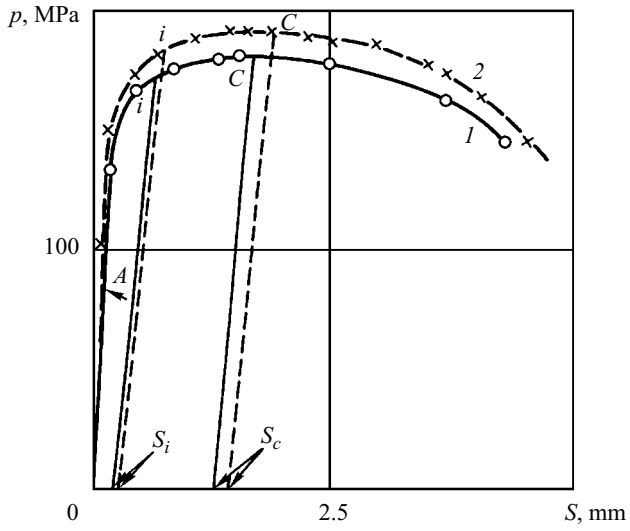

Fig. 26

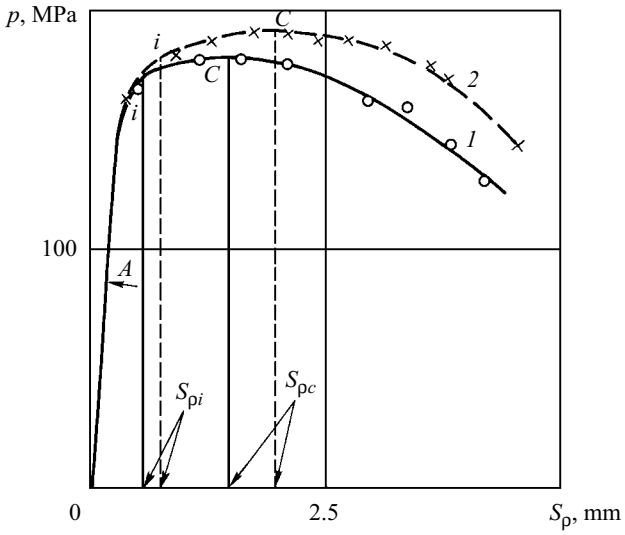

Fig. 27

TABLE 11

Material	Bulging	p_c, MPa	l_c, mm	K_c, MPa·$\sqrt{\text{m}}$				
				1	2	3	4	5
Steel N36	yes	349	53.0	155.2	167.4	170.2	171.2	171.9
	no	417	54.6	188.9	206.5	210.1	213.8	214.3
D16T	yes	146	54.2	69.8	78.1	80.9	81.6	81.9
	no	163	57.2	81.6	95.9	103.2	107.7	110.6

TABLE 12

Material	$2b$, mm	h, mm	l_0, mm	p_{m_1}, MPa	p_{m_2}, MPa	$\delta = \frac{p_{m_2} - p_{m_1}}{p_{m_2}}$, %
AMg6M	250	0.50	50.0	11.4	13.1	13.6
	250	0.50	41.5	129.0	149.0	13.4
	250	0.50	30.0	154.0	169.0	8.9
	250	0.50	19.5	151.0	163.0	7.4
	200	1.45	40.0	117.0	122.0	4.1
AMtsM	250	0.92	40.0	6.5	5.9	6.8
D16T	200	0.97	41.0	14.6	16.3	10.4
VT-1-0	160	1.01	42.5	20.3	21.1	3.8
Steel 20	250	0.52	42.0	17.6	18.6	5.3
Steel 08kp	200	1.03	40.0	15.3	16.7	8.4
Steel N36	250	0.43	39.5	34.9	41.7	16.3

TABLE 13

α	l_0 / b	$p_{m_1}(\alpha)$, MPa	$p_{m_2}(\alpha)$, MPa	δ, %
π/4	0.5	129.3	139.9	7.6
	0.4	139.4	149.5	6.8
	0.3	171.8	182.4	5.8
	0.2	180.9	191.8	5.7
	0.1	221.3	228.7	3.2
π/2	0.3	143.2	159.5	10.2
5π/12		152.1	167.0	8.9
π/3		163.8	177.0	7.5
π/6		192.0	202.7	5.3
π/12		219.2	219.2	0

The measured critical crack length l_c was used to compute the critical stress intensity factor K_c for plates of finite width by the method of successive approximations, the Irwin formula, with allowance for the increase in the crack length due to plastic deformation [46, 53]. The results are in Table 11. The buckling decreases K_c by 26% for the D16T plates and by 20% for the N36 plates. This allows us to estimate the error of K_c computed for buckled plates without considering the buckling.

3.2.4. Strength of Plates. Table 12 summarizes the values of the fracture stress p_m in the case of buckling (p_{m_1}) and no buckling (p_{m_2}).

As is seen, the buckling strongly reduces the strength of plates. The degree of this reduction depends on the geometrical and mechanical characteristics of plates: it increases with increase in l_0 and decrease in h. The maximum reduction in strength is observed for more elastic materials. The following expression obtained for AMg6M plates with h = 0.26, 0.34, 0.50, 0.90, 1.45 mm and $2l_0$ = 30, 60, 80, 120 mm describes the decrease in strength due to buckling [72–74, 82]:

$$p_{m_2} = p_{m_1}\left(1 - 0.000652 l_0 / h\right). \tag{3.7}$$

3.2.5. Fracture of Plates with Cracks and Crack-Like Defects under Various Loading Conditions. The influence of the crack and buckling in plates with inclined cracks on the fracture characteristics was analyzed in [72, 74]. As the crack angle α decreases, the crack growth rate v starts increasing after certain crack length and the critical crack length decreases. The buckling causes v to increase and l_c to decrease, the effect of buckling intensifying with increasing l_0 / b and α. No buckling occurred for small values of l_0 / b and α—it was preceded by fracture. Table 13 gives the maximum stresses $p_{m_1}(\alpha)$ (buckling is present) and $p_{m_2}(\alpha)$ (buckling is absent) for AMg6M plates with h = 0.47 mm and several values of α and l_0 / b. The buckling has a strong influence on $p_m(\alpha)$, the degree of this influence also depending on α and l_0 / b. As the angle α decreases, the stress $p_m(\alpha)$ increases, weakening the effect of buckling. When $\alpha = \pi / 12$, no buckling was observed—it was preceded by fracture.

The dependence of the fracture stress p_m on the along-crack load q was studied for cross-like plates with cracks under biaxial loading. Such a dependence is shown in Fig. 28 for some materials:

I: AMg6M plates with h = 0.48 mm and l_0/b = 0.31, 0.45, 0.57, 0.74, 0.85 (lines *1–5*);

II: St. 20 plates with h = 0.54 mm and l_0/b = 0.57;

III: VT-1-1 plates with h = 0.43 mm and l_0/b = 0.57; and

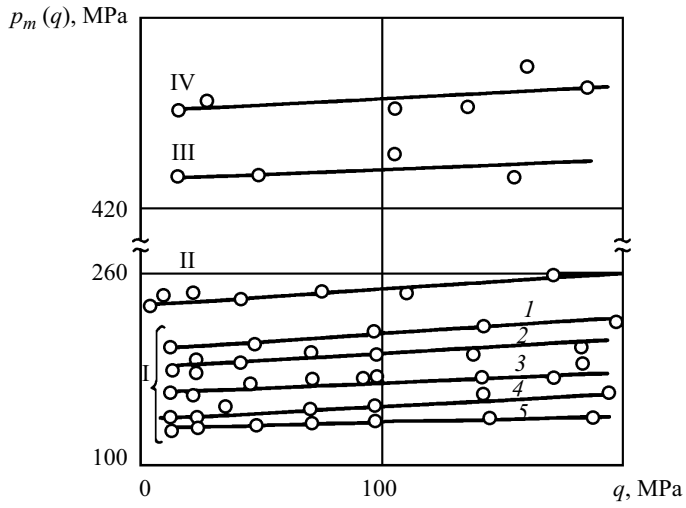

Fig. 28

TABLE 14

l_0 / b	q, MPa	$p_{m_1}(q)$, MPa	$p_{m_2}(q)$, MPa	δ, %
0.45	75.0	224.0	234.4	4.6
0.57	75.0	192.1	203.0	5.7
0.57	32.1	185.0	199.1	7.6
0.57	161.3	197.5	198.1	0.3
0.74	75.0	150.3	160.5	6.8
0.85	75.0	136.9	147.3	7.6

IV: St. N36 plates with h = 0.43 mm and l_0/b = 0.57.

It is seen that irrespective of the kind of the material and values of h and l_0 / b, high loads q do not cause $p_{m_1}(q)$ to increase considerably, which is consistent with linear fracture mechanics [36, 76].

The influence of buckling on the strength of plates is illustrated by Table 14. It presents the results of testing AMg6M plates with h = 0.48 mm (with buckling, $p_{m_1}(q)$, and without buckling, $p_{m_2}(q)$). It is seen that the effect of buckling depends on the values of l_0 / b and q. For example, if l_0 / b increases at q = const, then the deflection W and, consequently, δ increase too. If q decreases at l_0 / b = const, then the deflection W and, consequently δ increase.

Buckling in AMg6M plates with curved cracks increases the crack growth rate and reduces the strength. The degree of this reduction depends on the crack curvature: the greater the arc rise, the more the reduction at a given value of $2l_0$ [42]

The fracture of plates with a circular hole and two radial cracks was studied in [56, 72]. It has been established that the effect of buckling on the fracture characteristics depends on the mechanical and geometrical characteristics of plates such as the initial length $2l_0$ and radius R of the hole (the more the $2l_0$ at R = const and the less the R at $2l_0$ = const, the stronger the effect of buckling).

Figure 29 shows fracture curves for two-layer plates with $2l_0$ = 100 mm and h_1 = 0.53 mm, h_2 = 0.83 mm (curves I); h_1 = 0.53 mm, h_2 = 0.68 mm (curves II); and h_1 = 0.53 mm, h_2 = 0.10 mm (curves III) and for plates with h_1 = 0.53 mm, h_2 = 0.30 mm, and $2l_0$ = 60 mm (curves IV); $2l_0$ = 80 mm (curves V); and $2l_0$ = 100 mm (curve VI). Curves *1* and *2* refer to steel

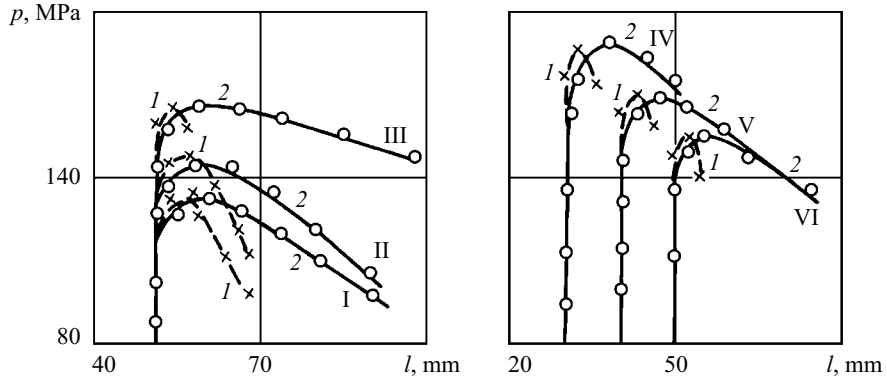

a b

Fig. 29

TABLE 15

$2l_0$, mm	h, mm	v, mm/sec		$\delta = \frac{v_2 - v_1}{v_1}$, %	p_m, MPa		$\delta = \frac{p_{m_2} - p_{m_1}}{p_{m_2}}$, %
		v_1	v_2		p_{m_1}	p_{m_2}	
100	0.63	1.12	1.24	10.1	185.1	166.4	10.1
	0.73	1.10	1.21	9.9	173.2	156.9	9.2
	0.83	1.05	1.15	9.5	165.7	153.3	7.5
	0.98	0.97	1.05	8.2	161.1	151.0	6.2
	1.21	0.85	0.92	8.1	151.1	142.1	6.0
	1.36	0.77	0.84	7.7	139.9	132.4	5.4
80	0.83	1.95	2.20	12.8	181.2	172.0	5.0
60	0.83	3.15	3.75	19.1	197.0	188.8	4.2

and aluminum, respectively. As is seen, initially, increasing load does not cause the crack to grow, and the fracture curves are similar to those for single-layer plates. The difference becomes noticeable with further loading [51, 88]. The crack starts growing earlier in the aluminum plate than in the steel one. The aluminum plates fracture much more intensively than the steel plates do; therefore, at the same level of stress p, the crack length l is much larger in the aluminum plate than in the steel one. When the aluminum plate is completely distructed, the steel plate still has load-bearing capacity. The behavior of the crack in the steel plate depends on the ratio of h_1 and h_2: the more the h_2, the greater the crack length l in the steel plate at the time of complete destruction of the aluminum plate. For example, at the time of fracture of the AMg6M plate, the crack length in the St. 20 plate was 10 mm in case III, 40 mm in case II, and 54 mm in case I. The difference in the behavior of cracks in steel and aluminum plates results in delamination of a two-layer plate along the crack path. The delamination zone expands as the crack grows. The delamination zones were different in size in different plates, which may apparently be attributed to the strength of the adhesive bond.

The kinetics of fracture and the strength of two-layer plates are characterized by the data in Table 15. The table collects the values of the crack growth rate v (v_1 in the case of buckling and v_2 in the case of no buckling) at crack length $l = 80$ mm (or crack length increment $\Delta l = 30$ mm). The value of δ characterizes the effect of buckling. As h and especially $2l_0$ decrease, the rate v increases. It is also greater in the presence of buckling. The buckled plates achieve a certain value of v at a smaller crack length l than the plates with no buckling do. The value of δ increases considerably with decrease in $2l_0$. Table 15 gives the maximum loads p_m in the absence (p_{m_1}) and presence (p_{m_2}) of buckling. As is seen, p_m decreases with increasing $2l_0$, which is due to the decrease in the plate section that runs through the crack and takes up the applied load. Also p_m decreases with increasing h. The

TABLE 16

l_0 / b	Δl, mm								
	v_{m_1}, mm/sec			v_{m_2}, mm/sec			v_{m_3}, mm/sec		
	20	40	50	20	40	50	20	40	50
0.32	2.45	1.95	0.75	2.40	2.80	2.50	0.85	1.10	1.25
0.43	1.70	0.55	0.25	1.60	0.70	0.45	0.90	1.40	1.70
0.57	0.25	0.40	0.15	0.45	0.20	0.15	1.55	4.55	6.50

TABLE 17

l_0 / b	p_{m_1}, MPa	p_{m_2}, MPa	δ_1, %	p_{m_3}, MPa	δ_2, %
0.3	95	103	8	129	36
0.4	64	72	13	107	67
0.5	33	44	33	87	164
0.6	13	30	131	73	469

reason is that the thickness h increases because of an increase in the thickness h_2 of the aluminum plate alone (the thickness h_1 remains the same). Though the load-bearing capacity of the plate increases with h, the stress p decreases, since the strength of the aluminum plate is less than that of the steel plate. The buckling reduces the maximum load, with δ depending on the geometrical and mechanical characteristics of the plate. The value of δ increases with increase in $2l_0$ and decrease in h. For specific characteristics of the tested plates, the maximum reduction in the load due to local buckling was about 10%.

The effects of buckling and loading conditions on the kinetics of fracture and the strength of plates with an edge crack was studied in [49, 50, 52, 82, 87, 89]. Table 16 gives v versus l_0/b for AMg6M plates. Here v_{m_1}, v_{m_2}, and v_{m_3} are the crack growth rates in the case of hinged application of load (in the presence of buckling), hinged application of load (no buckling), and direct application of load; and Δl is the crack length increment. The behavior of v is different in the cases of direct and hinged application of load. In the former case, v increases all the time, as in plates with a central crack, the rate of increase rising at some moment. This moment was considered the beginning of avalanche-like fracture. In the case of hinged application of load, no avalanche-like fracture was observed. At first the rate v increases and then, after reaching the maximum value, decreases. As the crack approaches the opposite edge of the plate, the crack growth rate decreases. The less the initial crack length, the more the maximum crack growth rate v_m. In the buckled plates, the crack starts growing under smaller load and the maximum crack growth rate is higher than in the plates with no buckling.

Table 17 shows the dependences of the fracture stress p_m on l_0 / b for AMg6M material. Here p_{m_1}, p_{m_2}, and p_{m_3} correspond to the cases of hinged application of load (in the presence of buckling), hinged application of load (no buckling), and direct application of load, and $\delta_1 = (p_{m_2} - p_{m_1}) / p_{m_1}$, $\delta_2 = (p_{m_3} - p_{m_1}) p_{m_1}$.

As is seen, the stress is maximum under directly applied load. An increase in l_0/b and buckling strongly reduce the maximum stress. The degree of reduction in strength due to hinged application of load in the presence of buckling and due to change of the way the load is applied in the absence of bulging depends on the ratio l_0 / b.

The strength of plates with an edge crack also depends on the crack angle α [83]. Figure 30 shows the dependence of the ratio p_{m_1} / p_{m_2} on the crack angle α at l_0 = 90 mm (curve *1*) and on the initial crack length l_0 at α = 30° (curve *2*). As is seen,

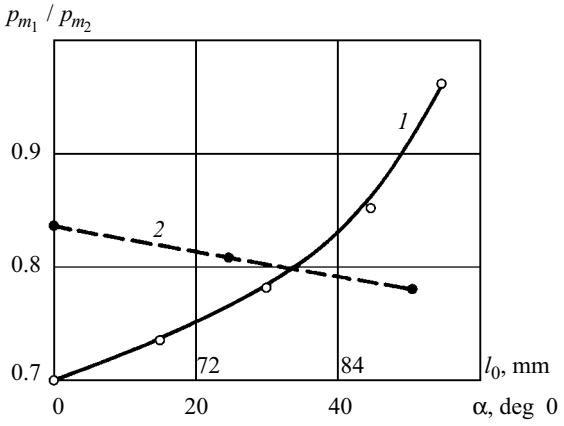

Fig. 30

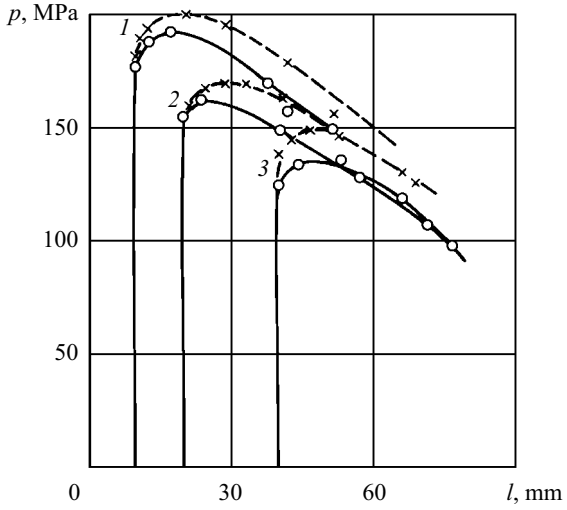

Fig. 31

increase in α and decrease in l_0 considerably weaken the effect of buckling on the strength of plates (the ratio p_{m_1} / p_{m_2} increases, i.e., p_{m_1} becomes closer to p_{m_2}). For l_0 = 90 mm, the maximum reduction in the strength of the tested plates was about 30% at α = 0 and the minimum reduction was about 4% at α = 55. For α = 30, the maximum reduction was 22% at l_0 = 90 mm and the minimum reduction was 16% at l_0 = 65 mm.

With the help of a TsDM PU-10 pulsator, the plates were subjected to cyclic tensile forces with a frequency of 14 Hz in the mode of asymmetric cycle with stress ratio r = 0.2 [43]. It has been established that at the equal number of cycles N, the crack growth rate v in buckled plates is higher by a factor of 2 to 5 (depending on the material of plates, the initial crack length, and the maximum cyclic stress p_m). The buckling reduces the endurance of plates, the degree of reduction increasing with $2l_0$ and p_m. The reduction in the endurance was about 48% in St. 20 plates with h = 0.78 mm, l_0 / b = 0.52, and p_m = 82 MPa and about 52% in VT-1-0 plates with h = 0.95 mm, l_0 / b = 0.56, and p_m = 52.6 MPa.

3.2.6. Fracture of Shells with Cracks. Figure 31 shows fracture curves for panels with radius R = 2000 mm and crack lengths $2l_0$ = 20, 40, 80 mm (curves *1–3*) [47, 72]. The solid curves refer to the case of free buckling and the dashed curves to the case of no buckling. A feature of these curves is that the load p that triggers postcritical fracture comprises about 30% of the load p_m. As $2l_0$ decreases, the loads p_i and p_m increase. These loads are much higher when there is no buckling. The effect of buckling on p_i and p_m depends on $2l_0$: as the crack grows, these stresses increase, reaching 15 and 17%, respectively. The stresses p_m and p_i were not observed to depend on the radius of panels. In the buckled panels, a certain crack growth rate v is achieved at a smaller crack length than in the panels with no buckling. Comparing the values of v at l = 100 mm shows that the crack growth rate decreases with increase in $2l_0$, and the buckling increases the crack growth rate by 25%.

The fracture of cylindrical shells with cracks was studied in [72, 86]. It has been established that an increase in the diameter of shells at constant crack length and a decrease in the crack length at constant diameter lead to an increase in the fracture stress. The buckling decreases the critical crack length l_c and appreciably reduces the strength of shells. The value of δ depends on the crack length and the diameter of shells: as $2l_0$ increases and D decreases, δ increases. In testing conic shells, it has been established that the effect of buckling on the fracture characteristics depends on the diameter and tapering angle of shells and crack length. For a shell with φ = 20° and $2l_0$ = 40 mm, we have l_c = 44 mm and p_c = 146 MPa in the presence of buckling and l_c = 53 mm and p_c = 161 MPa in the absence of buckling. The buckling reduces the residual strength of shells by approximately 16%.

Conclusions. The present paper describes a new untraditional approach to fracture problems for materials and structural members with cracks. The approach is based on the mechanism of local buckling near defects. According to the three-dimensional linearized theory of stability of deformable bodies, local instability near defects is considered to trigger fracture under along-crack compression. Fracture studies were conducted for compressible and incompressible bodies with an arbitrary elastic potential using the theories of large and small subcritical strains and for two wide classes of structural materials: composite and elastoplastic materials.

Studies into the fracture of structural members (plates and shells made of various structural materials) with cracks and crack-like defects under tension considered local buckling near defects, which precedes the fracture process and strongly affects the stress–strain state and fracture characteristics.

The main conclusions are the following:

1. The critical loading characteristics (compressive strains and stresses) corresponding to fracture onset depend on the physicomechanical characteristics of the material. The critical loads for an infinite material with coplanar cracks equal the critical load causing surface instability of a half-space and do not depend on the number, shape, and relative arrangement of coplanar cracks. The critical loads corresponding to the flexural and symmetric buckling modes for coplanar cracks coincide.

2. The critical loading characteristics for parallel cracks (in particular, a periodic series of cracks) are in many respects determined by the interaction of cracks. The critical loads strongly depend on the distance between parallel cracks, which allows us to consider that parallel cracks interact under along-crack compression (in contrast to coplanar cracks in an infinite material). The critical loads for closely spaced parallel cracks may be dozens of times smaller than those for a single crack in an infinite material. In this case, the flexural buckling mode is realized.

3. Approximate design models produce large errors, both quantitative (hundreds of percent) and qualitative (for example, the behavior of critical loading characteristics as functions of the stiffness characteristics of the composite components).

4. Local buckling of a structural member (plate or shell) near the crack may precede fracture at certain relations between the geometrical characteristics of the structural member (thickness, width, and crack length) and the mechanical characteristics of the material (elastic modulus, Poisson's ratio, plastic limit, and ultimate strength).

5. Altering the stress–strain state in a plate, near-crack buckling increases the stress and strain concentration factors. The shape of a crack-like defect and the type of load have a strong effect on the critical stress and buckling mode.

6. Buckling influences the fracture kinetics, crack resistance, and residual strength of structural members: increases the crack growth rate and decreases the stress causing the crack to grow and fracture stress. The effect of buckling depends on the geometrical and mechanical characteristics of plates and shells. It intensifies with increase in the crack length and decrease in the plate/shell thickness and is stronger in more elastic structural members.

REFERENCES

1. G. M. Bartenev and T. N. Khazanovich, "The law of highly elastic strains in cross-linked polymers," *Vysokomolek. Soed*., **2**, No. 1, 21–28 (1960).
2. V. L. Bogdanov, A. N. Guz, and V. M. Nazarenko, "Fracture of semiinfinite material with a circular surface crack in compression along the crack plane," *Int. Appl. Mech*., **28**, No. 11, 687–704 (1992).
3. V. L. Bogdanov, A. N. Guz, and V. M. Nazarenko, "Fracture of a half-space with a near-surface circular crack: Spatial nonaxisymmetric problem," *Dokl. AN SSSR*, **319**, No. 4, 835–839 (1991).
4. V. L. Bogdanov and V. M. Nazarenko, "Study of the compressive failure of a semi-infinite elastic meterial with a harmonic potential," *Int. Appl. Mech*., **30**, No. 10, 760–765 (1994).
5. V. L. Bogdanov and V. M. Nazarenko, "Compression of a composite along a near-surface macrocrack," *Mekh. Komp. Mater*., **30**, No. 3, 352–358 (1994).
6. V. V. Bolotin, "Delamination-like defects in composite structures," *Mekh. Komp. Mater*., No. 2, 239–255 (1984).
7. V. Yu. Gol'tsev, E. M. Morozov, and P. E. Nedoshivin, "Stability of a sheet sample with a crack under tension," *Zavod. Labor*., No. 1, 96–98 (1969).
8. A. N. Guz, *Brittle Fracture Mechanics of Prestressed Materials* [in Russian], Naukova Dumka, Kiev (1983).
9. A. N. Guz, "Fracture mechanics of solids in compression along crack (two-dimensional problem)," *Int. Appl. Mech*., **18**, No. 3, 213–224 (1982).
10. A. N. Guz, "Mechanics of fracture of solids in compression along cracks (three-dimensional problem)," *Int. Appl. Mech*., **18**, No. 4, 285–294 (1982).
11. A. N. Guz, "On a failure criterion for solids compressed along a crack: A plane problem," *Dokl. AN SSSR*, **259**, No. 6, 1315–1318 (1981).

12. A. N. Guz, "On a failure criterion for solids compressed along a crack: A spatial problem," *Dokl. AN SSSR*, **261**, No. 1, 42–45 (1981).
13. I. A. Guz and A. N. Guz, "Stability of two different half-planes in compression along interfacial cracks: Analytical solutions," *Int. Appl. Mech*., **37**, No. 7, 906–912 (2001).
14. A. N. Guz and M. Sh. Dyshel', "Deformation of plates with an edge crack in tension," *Int. Appl. Mech*., **31**, No. 11, 944–948 (1995).
15. A. N. Guz and M. Sh. Dyshel', "Fracture and stability of notched thin-walled bodies in tension (survey)," *Int. Appl. Mech*., **26**, No. 11, 1023–1042 (1990).
16. A. N. Guz, V. I. Knyukh, and V. M. Nazarenko, "Three-dimensional axisymmetric problem of fracture in material with two discoidal cracks under compression along the latter," *Int. Appl. Mech*., **20**, No. 11, 1003–1012 (1984).
17. A. N. Guz, V. I. Knyukh, and V. M. Nazarenko, "Delamination of composite materials under compression along internal and near-surface macrocracks," *Prikl. Mekh*., **22**, No. 11, 40–46 (1986).
18. A. N. Guz, V. I. Knyukh, and V. M. Nazarenko, "Fracture of ductile materials in compression along two parallel disk-shaped cracks," *Int. Appl. Mech*., **24**, No. 2, 112–118 (1988).
19. A. N. Guz, V. I. Knyukh, and V. M. Nazarenko, "Delamination of a composite compressed along two parallel macrocracks," *Fiz.-Khim. Mekh. Mater*., **23**, No. 1, 72–78 (1987).
20. A. N. Guz, G. G. Kuliev, and N. Zeinalov, "Bulging of a plate with a curvilinear hole under tension," *Izv. AN SSSR*, *Mekh. Tverd. Tela*, No. 2, 163–168 (1979).
21. A. N. Guz, G. G. Kuliev, and I. A. Tsurpal, "Theory of the rupture of thin bodies with cracks," *Int. Appl. Mech*., **11**, No. 5, 485–487 (1975).
22. A. N. Guz and V. M. Nazarenko, "The theory of near-surface delamination in composites compressed along macrocracks," *Mekh. Komp. Mater*., No. 5, 826–833 (1985).
23. A. N. Guz and V. M. Nazarenko, "Fracture of a material in compression along a periodic system of parallel circular cracks," *Int. Appl. Mech*., **23**, No. 4, 371–377 (1987).
24. A. N. Guz and V. M. Nazarenko, "Fracture mechanics of materials under compression along cracks (survey). Hyperelastic materials," *Prikl. Mekh*., **25**, No. 9, 3–32 (1989).
25. A. N. Guz and V. M. Nazarenko, "Fracture mechanics of materials under compression along cracks (survey). Structural materials," *Int. Appl. Mech*., **25**, No. 10, 959–972 (1989).
26. A. N. Guz and V. M. Nazarenko, "Fracture of a half-space with a surface disk-shaped crack: Axisymmetric problem," *Dokl. AN SSSR*, **274**, No. 1, 38–41 (1984).
27. A. N. Guz and V. M. Nazarenko, "Plastic near-surface fracture of materials compressed along macrocracks: Spatial problem," *Dokl. AN SSSR*, **284**, No. 4, 812–815 (1985).
28. A. N. Guz and V. M. Nazarenko, "Fracture of materials compressed along periodic cracks under plane strain," *Prikl. Mat. Mekh*., **51**, No. 2, 323–329 (1987).
29. A. N. Guz, V. M. Nazarenko, and S. M. Nazarenko, "Fracture of composites under compression along periodically placed parallel circular stratifications," *Int. Appl. Mech*., **25**, No. 3, 215–221 (1989).
30. A. N. Guz, V. M. Nazarenko, and I. P. Starodubtsev, "A planar problem of failure of structural materials in compression along two parallel cracks," *Int. Appl. Mech*., **27**, No. 4, 352–360 (1991).
31. A. N. Guz, V. M. Nazarenko, and I. Yu. Khoma, "Failure of an infinitely compressible composite containing a finite cylindrical crack in axial compression," *Int. Appl. Mech*., **31**, No. 9, 695–703 (1995).
32. A. N. Guz, V. M. Nazarenko, and I. Yu. Khoma, "Fracture of a composite compressed along a cylindrical crack," *Dop. NAN Ukrainy*, No. 10, 48–52 (1995).
33. M. M. Davidenkov, "Surface energy of mica," *Prikl. Mekh*., **6**, No. 2, 138–142 (1960).
34. Yu. N. Dal', "Local bending of a plate with a crack under tension," *Izv. AN SSSR*, *Mekh. Tverd. Tela*, No. 4, 135–141 (1978).
35. M. Sh. Dyshel', "Stability of thin plates with cracks under biaxial tension," *Int. Appl. Mech*., **18**, No. 10, 924–928 (1982).
36. M. Sh. Dyshel', "Buckling and fracture of plates with cracks under biaxial tension," *Prikl. Mekh*., **19**, No. 6, 107–110 (1983).
37. M. Sh. Dyshel', "Stability and fracture of a plate with two cracks under tension," *Prikl. Mekh*., **19**, No. 8, 113–118 (1983).

38. M. Sh. Dyshel', "Study into the deformation of a cylindrical shell near a slit under tension," *Prikl. Mekh*., **20**, No. 3, 108–110 (1984).
39. M. Sh. Dyshel', "Tension of a cylindrical shell with a slit," *Int. Appl. Mech*., **20**, No. 10, 941–945 (1984).
40. M. Sh. Dyshel', "Stability of thin plates with pointed holes under tension," *Prikl. Mekh*., **21**, No. 2, 119–123 (1985).
41. M. Sh. Dyshel', "Tension of a conic shell with a slit," *Prikl. Mekh*., **22**, No. 6, 121–124 (1986).
42. M. Sh. Dyshel', "Buckling and fracture of plates with curved cracks under tension," *Prikl. Mekh*., **23**, No. 8, 110–114 (1987).
43. M. Sh. Dyshel', "Local buckling of plates with cracks under cyclic loading," *Prikl. Mekh*., **24**, No. 6, 118–121 (1988).
44. M. Sh. Dyshel', "Influence of local buckling of plates with cracks on their crack resistance," *Prikl. Mekh*., **25**, No. 3, 126–129 (1989).
45. M. Sh. Dyshel', "Stability of a cracked cylindrical shell in tension," *Int. App. Mech*., **25**, No. 6, 542–548 (1989).
46. M. Sh. Dyshel', "Stress-intensity coefficient taking account of local buckling of plates with cracks," *Int. Appl. Mech*., **26**, No. 1, 87–90 (1990).
47. M. Sh. Dyshel', "Fracture of cylindrical panels with cracks under tension," *Prikl. Mekh*., **26**, No. 7, 63–67 (1990).
48. M. Sh. Dyshel', "Local stability loss and failure of cracked plates during the plastic deformation of materials," *Int. Appl. Mech*., **30**, No. 1, 44–47 (1994).
49. M. Sh. Dyshel', "Fracture of plates with an edge crack and local buckling under tension," *Prikl. Mekh*., **32**, No. 2, 59–63 (1996).
50. M. Sh. Dyshel', "Influence of plastic properties on the stability and fracture of plates with an edge crack," *Prikl. Mekh*., **34**, No. 7, 73–77 (1998).
51. M. Sh. Dyshel', "Fracture of two-layer plates with cracks and local buckling under tension," *Mekh. Komp. Mater*., **38**, No. 5, 663–672 (2002).
52. M. Sh. Dyshel', "Fracture and stability of plates with an edge crack under tension," *Dop. NAN Ukrainy*, No. 5, 39–41 (1995).
53. M. Sh. Dyshel', "Allowing for local buckling of plates with cracks in experimental determination of the intensity factor," *Dokl. AN USSR*, *Ser. A*, No. 11, 40–44 (1988).
54. M. Sh. Dyshel' and A. I. Zirka, "Stress state of a plate with a crack and local buckling under tension," *Prikl. Mekh*., **22**, No. 9, 120–124 (1986).
55. M. Sh. Dyshel', A. I. Zirka, and M. A. Mekhtiev, "Stress analysis of a plate with a hole and cracks reaching its boundary under tension with consideration of bulging," *Prikl. Mekh*., **23**, No. 7, 110–113 (1987).
56. M. Sh. Dyshel' and M. A. Mekhtiev, "Failure of tensioned plates weakened by a circular hole with radial cracks emanating from its contour," *Int. Appl. Mech*., **25**, No. 5, 490–494 (1989).
57. M. Sh. Dyshel' and O. B. Milovanova, "Local buckling of cylindrical panels with cracks under tension," *Prikl. Mekh*., **25**, No. 11, 123–126 (1989).
58. M. Sh. Dyshel' and O. B. Milovanova, "A method of experimentally analyzing the instability of plates with slits," *Int. Appl. Mech*., **13**, No. 5, 491–495 (1977).
59. V. I. Knyukh, "Fracture of a material with two disk-shaped cracks in the case of axisymmetric deformation in compression along the cracks," *Int. Appl. Mech*., **21**, No. 3, 226–231 (1985).
60. Z. N. Litvinenkova, "Stability of a plate with an internal crack under tension," *Izv. AN SSSR*, *Mekh. Tverd. Tela*, **5**, 148–151 (1973).
61. O. B. Milovanova and M. Sh. Dyshel', "Stability of thin sheets with an oblique slit in tension," *Int. Appl. Mech*., **16**, No. 4, 333–337 (1980).
62. V. M. Nazarenko, "Mutual effect of a circular surface crack and a free boundary in an axisymmetric problem of the fracture of an incompressible half space in compression along the crack plane," *Int. Appl. Mech*., **21**, No. 2, 133–138 (1985).
63. V. M. Nazarenko, "Plastic rupture of materials during compression along near-surface fractures," *Int. Appl. Mech*., **22**, No. 3, 245–250 (1986).
64. V. M. Nazarenko, "Fracture of materials compressed along near-surface cracks: Plane problem," *Prikl. Mekh*., **22**, No. 10, 72–81 (1986).

65. V. M. Nazarenko, “The theory of fracture of materials compressed along near-surface cracks: Plane strain case,” *Prikl. Mekh*., **22**, No. 12, 96–104 (1986).
66. V. M. Nazarenko, “Fracture of plastic masses with translational hardening under compression along near-surface macrocracks,” *Prikl. Mekh*., **23**, No. 1, 70–75 (1987).
67. V. M. Nazarenko, “Fracture of plastic masses with translational strain-hardening in compression along near-surface cracks,” *Int. Appl. Mech*., **25**, No. 1, 61–65 (1989).
68. V. M. Nazarenko, “Compression of a material along periodic parallel circular cracks: Spatial problem,” *Prikl. Mat. Mekh*., **52**, No. 1, 145–152 (1988).
69. V. M. Nazarenko, “Fracture of a half-space with a surface disk-shaped crack: Axisymmetric problem,” *Dokl. AN SSSR*, **274**, No. 1, 38–41 (1984).
70. V. M. Nazarenko and Yu. I. Khoma, “Method for solving fracture problems for an infinite material with a cylindrical crack under axial compression (the case of unequal roots),” *Dokl. AN Ukrainy*, No. 7, 62–67 (1994).
71. V. M. Nazarenko and Yu. I. Khoma, “Compression of an infinite composite along a finite cylindrical crack,” *Mekh. Komp. Mater*., **31**, No. 1, 27–34 (1995).
72. A. N. Guz, M. Sh. Dyshel’, and V. M. Nazarenko, *Fracture and Stability of Cracked Bodies*, Vol. 4 of the four-volume five-book series, A. N. Guz (general editor), *Nonclassical Problems of Fracture Mechanics* [in Russian], Naukova Dumka, Kiev (1992).
73. A. N. Guz, M. Sh. Dyshel’, G. G. Kuliev, and O. B. Milovanova, “Fracture and local instability of thin-walled bodies with notches,” *Int. Appl. Mech*., **17**, No. 8, 707–722 (1981).
74. A. N. Guz, M. Sh. Dyshel’, G. G. Kuliev, and O. B. Milovanova, *Fracture and Stability of Thin Bodies with Cracks* [in Russian], Naukova Dumka, Kiev (1981).
75. I. P. Starodubtsev, “Fracture of a body compressed along two parallel cracks: Plane strain case,” *Prikl. Mekh*., **24**, No. 6, 79–84 (1988).
76. A. N. Guz, M. Sh. Dyshel’, G. G. Kuliev, and É. N. Mamedov, “Theoretical and experimental investigation of plates with cracks under biaxial loading,” *Probl. Prochn*., No. 2, 3–5 (1982).
77. A. N. Guz, M. Sh. Dyshel’, N. K. Zeinalov, and G. G. Kuliev, “Theoretical and experimental investigation of a plate with a noncircular hole under tension,” *Dokl. AN USSR*, *Ser. A*, No. 2, 38–41 (1980).
78. A. N. Guz, M. Sh. Dyshel’, G. G. Kuliev, and O. B. Milovanova, “Stability of thin plates with cracks,” *Dokl. AN USSR*, *Ser. A*, No. 5, 421–426 (1977).
79. G. P. Cherepanov, “Bulging of membranes with a hole under tension,” *Prikl. Mekh. Mat*., **27**, No. 2, 275–286 (1963).
80. V. L. Bogdanov, A. N. Guz, and V. M. Nazarenko, “Nonaxisymmetric compressive failure of a circular crack parallel to a surface of half-space,” *Theor. Appl. Fract. Mech*., **22**, 239–247 (1995).
81. M. Sh. Dyshel’, “Local buckling of extended plates containing cracks and crack-like defects, subject to the influence of geometrical parameters of the plates and the defects,” *Int. Appl. Mech*., **35**, No. 12, 1272–1276 (1999).
82. M. Sh. Dyshel’, “Stability and fracture of plates with a central and an edge crack under tension,” *Int. Appl. Mech*., **38**, No. 4, 472–476 (2002).
83. M. Sh. Dyshel’, “Fracture of plates with an inclined edge crack under tension,” *Int. Appl. Mech*., **40**, No. 5, 580–582 (2004).
84. M. Sh. Dyshel’, “Stability of plates with an oblique edge crack under tension,” *Int. Appl. Mech*., **39**, No. 9, 1081–1083 (2003).
85. E. Yu. Gladun, A. N. Guz, and Yu. V. Kokhanenko, “Estimating the error of the beam approximation in the plane stability problem for a rectangular plate with a central crack,” *Int. Appl. Mech*., **40**, No. 11, 1290–1296 (2004).
86. A. N. Guz, “Design models in linearized solid mechanics,” *Int. Appl. Mech*., **40**, No. 5, 506–516 (2004).
87. A. N. Guz and M. Sh. Dyshel, “Fracture of cylindrical shells with cracks in tension,” *Theor. Appl. Fract. Mech*., No. 4, 123–126 (1985).
88. A. N. Guz and M. Sh. Dyshel, “Fracture and buckling of thin panels with edge crack in tension,” *Theor. Appl. Fract. Mech*., No. 36, 57–60 (2001).
89. A. N. Guz and M. Sh. Dyshel, “Buckling and cracking characteristics of two-layered plate in tension,” *Theor. Appl. Fract. Mech*., No. 38, 103–107 (2002).

90. A. N. Guz and M. Sh. Dyshel, “Stability and residual strength of panels with straight and curved cracks,” *Theor. Appl. Fract. Mech*., No. 41, 95–101 (2004).
91. A. N. Guz, Yu. I. Khoma, and V. M. Nazarenko, “On fracture of an infinite elastic body in compression along a cylindrical defect,” in: *Advance in Fracture Research*, *Proc. 9th Int. Conf. on Fracture*, Sydney, Australia, 4 (1999), pp. 2047–2054.
92. A. N. Guz, V. I. Knukh, and V. M. Nazarenko, “Compressive failure of material with two parallel cracks: small and large deformation,” *Theor. Appl. Fract. Mech*., **11**, No. 3, 213–223 (1989).
93. A. N. Guz and V. M. Nazarenko, “Symmetric failure of the half-space with penny-shaped cracks in compression,” *Theor. Appl. Fract. Mech*., **3**, No. 3, 233–245 (1985).
94. A. N. Guz, V. M. Nazarenko, and I. P. Starodubtsev, “On problems of fracture of materials in compression along two internal parallel cracks,” *Appl. Math. Mech*., **18**, No. 6, 517–528 (1997).
95. F. John, “Plane strain problems for a perfectly elastic material of harmonic type,” *Comm. Pure Appl. Math*., **13**, No. 2, 239–296 (1960).
96. I. W. Obreimoff, “The splitting strength of mica,” *Proc. Royal Soc. London*, *A*, **127**, 290–297 (1930).
97. L. R. G. Treloar, “Large elastic deformations in rubber-like materials,” in: *IUTAM Colloq*., Madrid (1955), pp. 208–217.